Journal of Medicinal Chemistry

Article

pubs.acs.org/jmc

4,6-Diphenylpyridines as Promising Novel Anti-Influenza Agents Targeting the PA−PB1 Protein−Protein Interaction: Structure−Activity Relationships Exploration with the Aid of Molecular Modeling

Iuni M. L. Trist,[†,#] Giulio Nannetti,[‡,#] Cristina Tintori,[†] Anna Lucia Fallacara,[†] Davide Deodato,[†] Beatrice Mercorelli,[‡] Giorgio Palù,[‡] Maikel Wijtmans,[§] Tzveta Gospodova,[∥] Ewald Edink,[§] Mark Verheij,[§] Iwan de Esch,[§] Lilia Viteva,[∥] Arianna Loregian,*[,‡,#,○] and Maurizio Botta*[,†,⊥,#,▽]

[†]Dipartimento di Biotecnologie, Chimica e Farmacia, Università degli Studi di Siena, Via A. Moro, I-53100 Siena, Italy

[‡]Dipartimento di Medicina Molecolare, Università degli Studi di Padova, Via A. Gabelli 63, I-35121 Padova, Italy

[§]Division of Medicinal Chemistry, Amsterdam Institute for Molecules, Medicines and Systems, VU University Amsterdam, De Boelelaan 1083, 1081 HV Amsterdam, The Netherlands

[∥]Institute of Organic Chemistry with Centre of Phytochemistry, Bulgarian Academy of Sciences, Acad. Georgy Bonchev str. Bl. 9, 1113 Sofia, Bulgaria

[⊥]Sbarro Institute for Cancer Research and Molecular Medicine, Temple University, BioLife Science Building, Suite 333, 1900 N 12th Street, Philadelphia, Pennsylvania 19122, United States

Supporting Information

ABSTRACT: Influenza is an infectious disease that represents an important public health burden, with high impact on the global morbidity, mortality, and economy. The poor protection and the need of annual updating of the anti-influenza vaccine, added to the rapid emergence of viral strains resistant to current therapy make the need for antiviral drugs with novel mechanisms of action compelling. In this regard, the viral RNA polymerase is an attractive target that allows the design of selective compounds with reduced risk of resistance. In previous studies we showed that the inhibition of the polymerase acidic protein-basic protein 1 (PA−PB1) interaction is a promising strategy for the development of anti-influenza agents. Starting from the previously identified 3-cyano-4,6-diphenyl-pyridines, we chemically modified this scaffold and explored its structure−activity relationships. Noncytotoxic compounds with both the ability of disrupting the PA−PB1 interaction and antiviral activity were identified, and their mechanism of target binding was clarified with molecular modeling simulations.

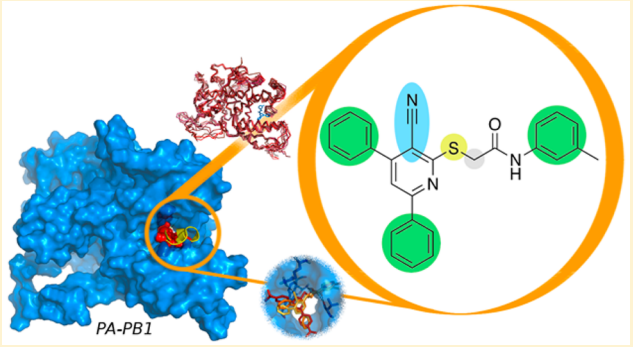

INTRODUCTION

Despite the efforts in antiviral research, influenza (Flu) is an infectious disease that still represents an important public health burden affecting 5−10% of the World's population, resulting in 3−5 million severe cases and in 250−500 thousands deaths each year.[1] It is caused by the ribonucleic acid (RNA) viruses of the *Orthomyxoviridae* family, and they are classified in A, B, and C according to their antigenic differences.[2−4] Among these, influenza A virus (FluA) infects a variety of animals as well as humans. Hemagglutinin (HA) and neuraminidase (NA) are the two major viral antigenic glycoproteins, and the 18 HA (H1−H18) and 11 NA (N1−N11) identified in FluA virus result in the generation of distinct viral subtypes.[5] Some of them are responsible for severe upper respiratory diseases in humans that occur in both seasonal epidemics and sporadic pandemics associated with high morbidity and mortality. Millions of deaths were recorded in the most important pandemics of the last century.[6,7] In chronological order, these were the Spanish Flu (H1N1 strain, in 1918),[8,9] the Asian Flu (H2N2 strain, in 1957),[9] the Hong Kong Flu (H3N2 strain, in 1968),[9] and the "swine" Flu (H1N1 strain, in 2009).[10] Recently, the zoonotic infection caused by the "avian" FluA subtype H7N9 registered a fatality rate of 25% of the confirmed cases. In this outbreak, it was proven that most of the patients were directly infected from poultry, although the existence of limited human-to-human spread could not be excluded. However, the possibility of sustained

Received: December 15, 2015
Published: February 29, 2016

DOI: 10.1021/acs.jmedchem.5b01935
J. Med. Chem. 2016, 59, 2688−2703

acquisition of human-to-human transmission capabilities by this pathogen could result in a devastating worldwide health problem, raising much concern for its pandemic potential.[11]

Reassortments of the genetic material between different strains allow the virus to avoid host detection systems and the emergence of the extremely aggressive viruses responsible for the pandemics. These, antigenic drift in particular, are complicating factors hampering the development of an effective and universal anti-Flu vaccine, and thus, the development of anti-influenza drugs is essential for the fight of future Flu outbreaks.[12,13] Clinical therapy relies only on two classes of drugs that inhibit either the M2 ion channel (amantadine and rimantadine) or NA (e.g., oseltamivir and zanamivir).[14,15] M2 ion channel inhibitors were the first anti-influenza drugs approved. However, they are no longer recommended due to their serious side effects on the central nervous system (CNS) and the very rapid emergence of drug-resistant influenza strains.[14−16] Furthermore, drug-resistant FluA viruses are also emerging for the current first line therapy (NA inhibitors), making the discovery of novel antiviral strategies essential.[14,15,17,18]

A new molecular target that was identified in the past few years is FluA RNA-dependent RNA polymerase (RdRp), a protein complex essential for the viral replication and pathogenesis. Indeed, it is responsible for viral RNA replication and an endonuclease activity for the "cap-snatching", which is necessary for both transcription initiation and translation.[19] Importantly, FluA RdRp is significantly different from human polymerases and it is highly conserved among the different Flu subtypes, facilitating the design of selective compounds with reduced probability of virus resistance development. RdRp is a complex of three virus-encoded subunits: the polymerase acidic protein (PA), the polymerase basic protein 1 (PB1), and the polymerase basic protein (PB2). Only the correct assembly of the three subunits allows the correct functioning of the enzyme.[19−23] Thus, an attractive mechanism of FluA RdRp inhibition is the disruption of the PA−PB1 protein−protein interaction. This is a very promising strategy for anti-influenza drug discovery, as demonstrated by the emergence of protein−protein interaction (PPI) small-molecule inhibitors in recent years.[14,15,24−36] Among these, a hit compound disrupting the PA−PB1 interaction was identified through a high-throughput docking as a potential FluA polymerase inhibitor and from this encouraging result a small library of purchased analogues was evaluated. With IC_{50} values in the micromolar range, the activity related to the 3-cyano-4,6-diphenyl-pyridine scaffold was confirmed as being responsible for the disruption of the PA−PB1 complex through the interaction of these molecules with the C-terminal domain of PA, mimicking the hydrophilic N-terminal portion of PB1 (residues 1−4).[35] In order to obtain a better understanding of the structure−activity relationship (SAR) of this promising class of compounds and aiming the improvement of their activity, a hit optimization process was performed in the study presented here.

RESULTS AND DISCUSSION

Hit Exploration. Starting from a simplified structure (compound **1**) of the novel class of inhibitors identified in the previous virtual screening campaign,[35] a series of analogues was designed for a better understanding of the underlying structure−activity relationships. The 3-cyano-4,6-diphenyl-pyridine scaffold was systematically modified by either removing or replacing molecule portions. Furthermore, attempts to increase compound solubility (e.g., **2**), to address the possibility of a covalent interaction between the protein and the thioether (e.g., **5** and **6**), and to increase the synthetic feasibility (e.g., **14** and **15**) were considered. All the synthesized compounds can be found in Table 1.

Chemistry. Due to the removing and replacing strategy adopted in the design of the molecules, several synthetic routes were applied. However, 2-chloro-4,6-diphenylnicotinonitrile (**16**) was used as a common precursor for the synthesis of several compounds (**1**, **3**−**8**, and **10**), as shown in Scheme 1. Of these, **1**, **3**, **4**, **7**, and **8** were obtained by nucleophilic aromatic substitution using the appropriate nucleophile (compounds **17a**−**e**). Reaction conditions differed according to the reactant properties, and in several cases, temperature control was important in order to avoid the formation of a highly fluorescent ring-closed side product. Extensive analysis was performed to confirm the regiochemistry of these reactions. An efficient Heck coupling reaction between *N*-(*m*-tolyl)-acrylamide (**18**) and precursor **16** was performed for the synthesis of compound **6**, which has a *trans* stereochemistry as indicated by the large *J* constant between the two vinylic protons (14.8 Hz). This alkene was then reduced to the saturated analogue **5**. Compound **10** was synthesized by hydrogenolysis of the C−Cl bond of compound **16**.

Precursors **17d** and **17e** were prepared through the neat acylation of 3-methyl-aniline (**19**) with either mercapto-propionic acid (**20**) or dihydrothiophen-2(3*H*)-one (**21**), respectively (Scheme 2). Intermediate **18** was obtained through the acylation of 3-methyl-aniline (**19**) with acryloyl chloride (**22**, Scheme 2).

Final products **12**, **13**, **14**, and **15** were synthesized by aromatic nucleophilic substitution on the appropriate aromatic electrophile **23a**−**d** with the nucleophile 2-mercapto-*N*-(*m*-tolyl)acetamide (**17a**) in acetonitrile, as shown in Scheme 3.

A different synthesis approach was required for compound **11**. As shown in Scheme 4, the pyridone **24** was chlorinated with $POCl_3$ to yield 2-chloro-4,6-diphenylpyridine (**25**), which then reacted with thiol (**17a**) through a Cu-catalyzed aromatic nucleophilic substitution, giving the final product (**11**).

Scheme 5 reports the synthetic strategy used for compounds **2** and **9**. The precursor 2-chloro-1-morpholinoethanone (**28**) was synthesized through the reaction of morpholine (**26**) with chloroacetyl chloride (**27**). Then, 4,6-diphenylpyridine-2-thiol (**29**) was used as a nucleophile in the nucleophilic substitution on **28** or iodomethane for the synthesis of the final products **2** and **9**, respectively.

Biological Evaluation of the Compounds. All the synthesized molecules were evaluated for their inhibitory activity against the PA−PB1 interaction. The abilities of the test compounds to inhibit the physical interaction between PA and PB1 and to block Flu virus replication were tested in enzyme-linked immunosorbent assays (ELISA) and in plaque reduction assays (PRA) in Mardin−Darby canine kidney (MDCK) cells infected with FluA virus (A/PR/8/34 strain), respectively. In order to exclude the possibility that the observed antiviral activity might be due to toxic effects on the infected cells, compound cytotoxicity was also assessed in two cell lines (MDCK and human embryonic kidney, HEK 293T) by the MTT assay. In these studies, the $PB1_{(1-15)}$-Tat peptide[37] was used as a positive control for inhibition in the ELISA, while the broad-spectrum inhibitor of RNA viruses polymerases Ribavirin (RBV)[38] was used as a positive control in the PRA as it inhibits viral polymerases, even though its mechanism of

DOI: 10.1021/acs.jmedchem.5b01935
J. Med. Chem. 2016, 59, 2688−2703

Scheme 1. Synthesis of Compounds 1, 3−8, and 10[a]

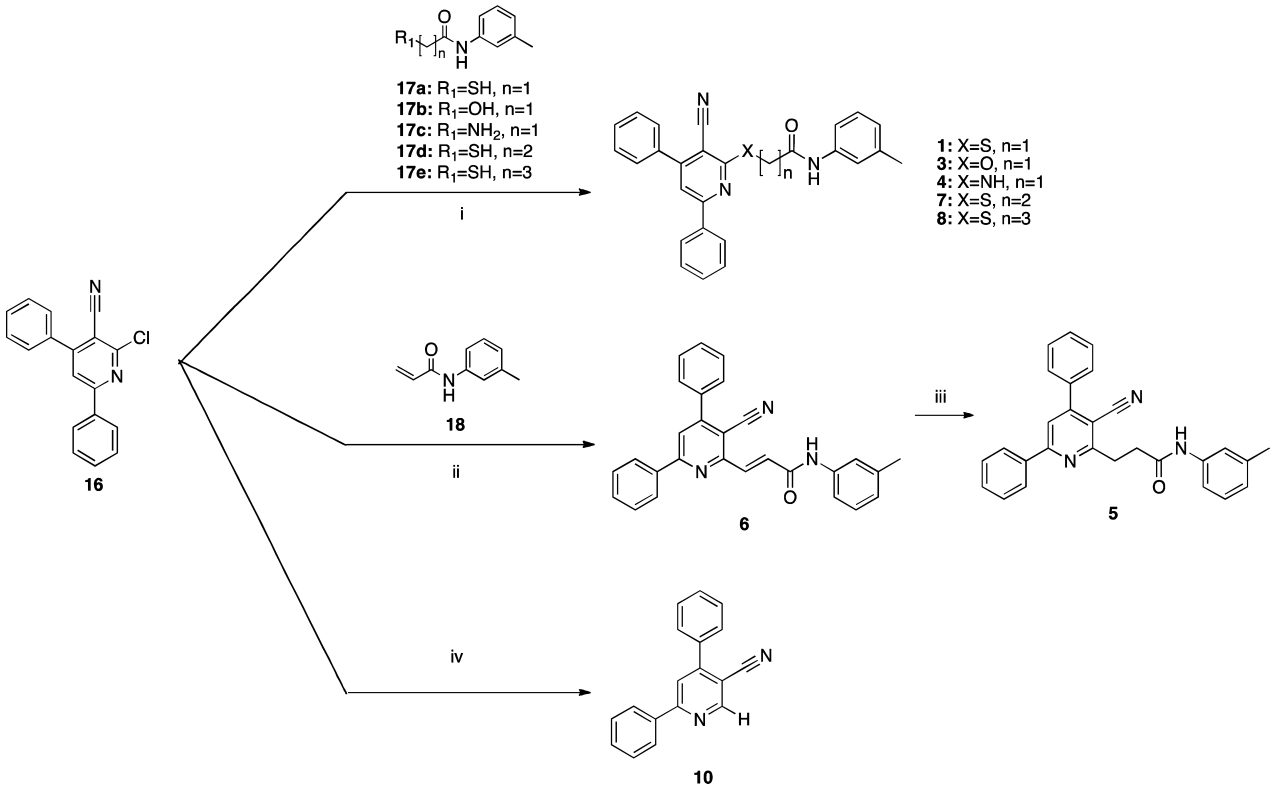

[a]Reagents and conditions: (i) DMF, K_2CO_3, rt, 1 h (for **1**); MeCN, CuI, Cs_2CO_3, MWO 120 °C, 1.5 h (for **3**); DMF, K_2CO_3, 45 °C, 18 h (for **4**); MeCN, K_2CO_3, 0 °C, 0.5 h then: rt, 3 h (for **7** and **8**); (ii) DMF, $Pd(OAc)_2$, TBAB, $(o\text{-tol})_3P$, NaOAc, 145 °C, 18 h; (iii) EtOAc, H_2, Pd/C, rt, 11 h; (iv) NaOAc, MeOH, H_2, $PdCl_2$, rt, 36 h.

action does not involve the inhibition of PA−PB1 formation. Moreover, the first line therapeutic NA inhibitor Oseltamivir (OSV)[39] was included as a positive control in the PRA. The results of the experiments are shown in Table 1. Most importantly, data revealed for the first time not only that the chemical scaffold studied in this hit optimization process is able to inhibit the formation of the FluA PA−PB1 complex with comparable IC_{50} with respect to the control ($PB1_{(1-15)}$-Tat peptide), but also that it exhibits a good cytotoxicity profile and a low micromolar antiviral activity, comparable to RBV. Despite less efficient antiviral activity was recorded for our compound family with respect to OSV, the family of compounds presented here inhibits a target that is less-prone to mutations than NA, for which resistance has frequently already emerged.

Lower activity in the ELISA experiments compared to the PRA could be observed, in particular for compounds **1**, **4**, **14**, and **15**. Compounds **1** and **14** exhibited a low-micromolar EC_{50} value in PRA (9.2 and 3.5 μM, respectively) and a 19−47-fold higher IC_{50} value in ELISA (175 and 165 μM, respectively), while **4** and **15** presented an EC_{50} around 30 μM in PRA (28.6 and 26.5 μM, respectively) and complete loss of the ability to disrupt the PA−PB1 interaction in ELISA. In order to investigate whether this could be due to the assay conditions, the ELISA was repeated for all molecules with EC_{50} values below 30 μM (**1**, **4**, **8**, **11**, **14**, and **15**). In this assay (henceforth mentioned as "Modified ELISA PA−PB1 Interaction Assay"), compounds were dissolved in a similar medium to the one used in the cell-based assays instead of the PBS buffer (see Experimental Section). Similarly to the previous ELISA PA−PB1 Interaction Assay, the $PB1_{(1-15)}$-Tat peptide[37] was used as

Scheme 2. Synthesis of Precursors 17d, 17e, and 18[a]

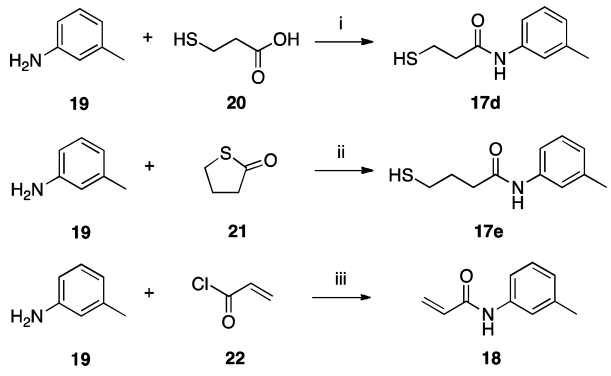

[a]Reagents and conditions: (i) rt, 1 h, then MWO, 180 °C, 1 h; (ii) MWO 120 °C → 240 °C, 28 h; (iii) TEA, THF, 0 °C, 2.5 h.

a positive control for inhibition. As reported in Table 2, a significant improvement in the inhibitory activity was obtained mainly for **1** and **15**, which were more soluble in the DMEM serum-free buffer with respect to the PBS one, while more modest improvements were obtained for **11** and **14**. The same IC_{50} values were registered for compounds **4** and **8**. As expected, comparable IC_{50} values were also obtained for the $PB1_{(1-15)}$-Tat peptide in the two assay conditions, suggesting that the medium was affecting the behavior of some of our compounds rather than the accessibility of the target site.

Data presented in both Table 1 and Table 2 are of great value for the understanding of the general mechanism of action of the 3-cyano-4,6-diphenyl-pyridine scaffold. A significant decrease in

DOI: 10.1021/acs.jmedchem.5b01935
J. Med. Chem. 2016, 59, 2688−2703

Scheme 3. Synthesis of Compounds 12, 13, 14, and 15[a]

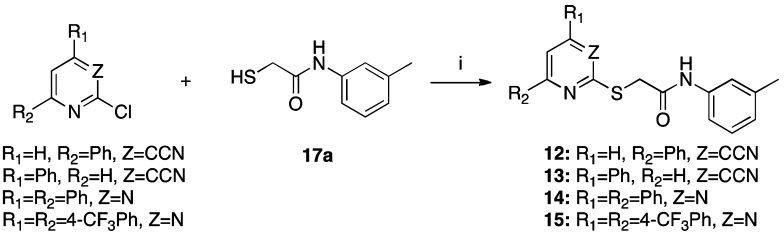

23a: R_1=H, R_2=Ph, Z=CCN
23b: R_1=Ph, R_2=H, Z=CCN
23c: R_1=R_2=Ph, Z=N
23d: R_1=R_2=4-CF_3Ph, Z=N

17a

12: R_1=H, R_2=Ph, Z=CCN
13: R_1=Ph, R_2=H, Z=CCN
14: R_1=R_2=Ph, Z=N
15: R_1=R_2=4-CF_3Ph, Z=N

[a]Reagents and conditions: (i) MeCN, K_2CO_3, rt, 30 min (for **12**); MeCN, NaOAc, rt, 18 h then 40 °C, 5 d (for **13**); MeCN, K_2CO_3, rt, 5 h (for **14**); MeCN, K_2CO_3, 0 °C to rt, 2.5 h (for **15**).

activity was observed in the attempts of substituting the sulfur atom (**3**, **4**, **5**, and **6**), indicating the importance of this heteroatom. Only for compound **4** the antiviral activity was partially retained. The whole sulfur-containing side chain appears to be also essential as its complete (**10**) or its partial (**9**) removal resulted in a reduction or a complete loss of activity. Nevertheless, a mild antiviral activity was observed for compound **10**. However, considering its significant cytotoxicity in MDCK cells and the high IC_{50} value in ELISA, its antiviral activity in PRA might be related to cell toxicity rather than to the inhibition of PA−PB1 interaction. This hypothesis is in keeping with the observation that the compound **10** lacks of one of the interaction with a relevant hydrophobic area within the PA binding region. Only one methylene group should be placed between the sulfur atom and the carbonyl moiety, as the extension of the chain (**7** and **8**) increased cytotoxicity. Furthermore, the 3-methyl substituted phenyl ring cannot be replaced by a more hydrophilic group, as indicated by the increased EC_{50} value of compound **2**. Given the inactivity and the higher cytotoxicity of **12** and **13**, the two phenyl rings directly attached to the pyridine ring (in positions 4 and 6) appear to be essential in the molecular scaffold. Interestingly, the removal of the cyano moiety linked to the same central core (**11**) did not affect activity. Good antiviral activity was observed also with the substitution of the pyridine ring with a pyrimidine one (**14**), but a lower ability to dissociate the PA−PB1 complex and a higher cytotoxicity were detected as well. However, this toxicity decreased with the introduction of two electron withdrawing CF_3 groups in the structure (**15**). For this compound, a better IC_{50} value was obtained in the modified ELISA, but a worse antiviral activity profile in respect to compounds **1**, **8**, **11**, and **14** was also detected.

From these results, compounds **1**, **11**, and **15** emerged as the most promising molecules since they display micromolar inhibition of the PA−PB1 interaction (with IC_{50} values ranging from 35.2 to 64.5 μM), interesting antiviral activity, and a good cytotoxicity profile with a selectivity index (SI) higher than 9.4. Among the other compounds, **4** showed an antiviral activity comparable to **15** and a good cytotoxicity profile (SI > 8.7), but no inhibition of the PA−PB1 interaction. Thus, aiming to better understand the mechanism of action of these compounds, the ability of **1**, **4**, **11**, and **15** to inhibit FluA RNA-dependent RNA polymerase (RdRp) enzymatic activity in a cellular context was assessed by minireplicon assays in transfected HEK 293T cells, using RBV[38] as a reference inhibitor. The results are presented in Table 3. All of the tested compounds were found to inhibit the viral polymerase activity, with encouraging EC_{50} values for compounds **11** and **15** (22.0 to 30.8 μM) in particular. Furthermore, from the results it emerges that probably compound **1**, in addition to the inhibition of the PA−PB1 interaction, might be involved in other mechanisms of action not related to the viral polymerase activity because its low EC_{50} value in the PRA assay (9.2 μM) does not reflect completely the activity in the minireplicon assay (EC_{50} 86.6 μM). Compound **4** inhibited the catalytic activity of the viral RdRp in the 293T cells (EC_{50} 46.3 μM), indicating that this molecule might exert its antiviral effects by inhibiting the viral RdRp activity, but through a mechanism of action that likely does not involve the PA−PB1 complex disruption.

The ability of these compounds to inhibit the polymerase activity in cells as well as the PA−PB1 interaction and the formation of viral plaques is a substantial indication that the most promising 4,6-diphenylpyridine (or pyrimidine) molecules exert their anti-influenza activity through the disruption of the PA−PB1 complex.

Molecular Modeling. In order to rationalize the SARs, all the synthesized compounds were examined by means of docking simulations within the PB1-binding site of PA in order to produce their putative binding poses.

The 3-cyano-4,6-diphenylpyridine series was discovered with a previous high-throughput docking study performed on a homology model built using the FluA H1N1 sequence and two PA−PB1 complexes templates (PDB IDs: 2ZNL[20] and 3CM8[21]).[35] Subsequent to the publication of the manuscript by Tintori et al.,[35] a novel X-ray structure of FluA H17N10 RdRp was published (PDB ID: 4WSB)[23] and comprised the whole PA in complex with PB1, PB2, and a viral RNA promoter. Since the C-terminal portion of PA (PAC) in 4WSB is more complete than the structures used to build the PA−PB1 complex *in silico* (2ZNL and 3CM8), the two PAC were compared in order to assess the quality of the homology model. The two structures have 71.21% identity in sequence alignment, and they superpose very well (RMSD 1.09 Å). Remarkably, the superposition is even better in the PB1-binding site region (RMSD of 0.537 Å), validating the reliability of the homology model. The backbone superposition of the homology model and PDB ID 4WSB is shown in Figure S1 of the Supporting Information. Since biological evaluations were performed on the FluA H1N1 strain and since the homology model was assessed of good quality, for consistency purposes, the homology model was used for the docking simulations.

Similarly to the procedure applied in the previous study,[35] docking simulations were carried out with two widely used programs (Glide[40] and GOLD[41]) and the binding poses were then compared. Most importantly, only the active compounds reproduced the already reported binding model[35] of the 3-cyano-4,6-diphenyl-pyridine derivatives, confirming the proposed mode of binding of this class of inhibitors. The pose obtained for compound **1** is shown in Figure 1 as an example.

DOI: 10.1021/acs.jmedchem.5b01935
J. Med. Chem. 2016, 59, 2688−2703

Table 1. Structure and Biological Activity of the Synthesized Compounds

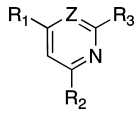

Compd	R_1	R_2	R_3	Z	ELISA PA-PB1 Interaction Assay IC_{50} (μM)[a]	PRA in MDCK cells EC_{50} (μM)[b]	Cytotoxicity (MTT assay)[c] HEK 293T cells CC_{50} (μM)[d]	Cytotoxicity (MTT assay)[c] MDCK cells CC_{50} (μM)[e]	SI[f]
1			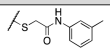	CCN	175 ± 22	9.2 ± 0.7	>250	>250	>27.2
2			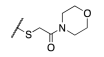	CCN	177 ± 20	100 ± 9	184 ± 14	>250	>2.5
3			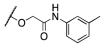	CCN	>200	93.9 ± 7.8	>250	>250	>2.7
4			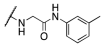	CCN	>200	28.6 ± 4.9	>250	>250	>8.7
5			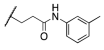	CCN	>200	>100	140.0 ± 7.8	>250	NC
6			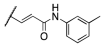	CCN	190 ± 31	70.7 ± 5.7	>250	>250	>3.5
7			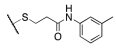	CCN	122 ± 19	>10[g]	150 ± 14	13.9 ± 2.0	NC
8			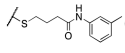	CCN	140 ± 22	8.2 ± 1.1	95.6 ± 15.8	41.5 ± 5.4	5.1
9				CCN	195 ± 15	>50[g]	144 ± 22	125 ± 16	NC
10			H	CCN	116 ± 26	45.1 ± 3.0	>250	105 ± 7	2.3
11			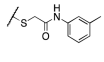	CH	52.6 ± 9	7.3 ± 1.3	>250	150 ± 19	20.5
12	H		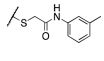	CCN	>200	>10[g]	32.0 ± 3.6	7.1 ± 1.1	NC
13		H	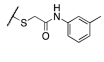	CCN	>200	>10[g]	180 ± 5	41.5 ± 4.2	NC
14			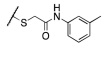	N	165 ± 18	3.5 ± 0.5	22.3 ± 1.8	10.1 ± 1.7	2.9
15				N	>200	26.5 ± 4.3	>250	>250	>9.4
RBV					ND	12.8 ± 2.1	>250	>250	>19.5
OSV					ND	0.015 ± 0.006	>250	>250	>16000
$PB1_{(1-15)}$–Tat peptide					35.9 ± 5.6	49.7 ± 5.1	>250	>250	>5.0

[a]Activity of the compounds in the ELISA PA–PB1 interaction assays. Values represent the compound concentration (in μM) that reduces the interaction between PA and PB1 by 50% (IC_{50}). [b]Antiviral activity of the compounds in plaque reduction assays against the Flu A/PR/8/34 strain. Values represent the compound concentration (in μM) that inhibits 50% of plaque formation (EC_{50}). [c]Cytotoxicity of the compounds exhibited in the MTT assays. Values represent the compound concentration (in μM) that causes a 50% decrease in cell viability (CC_{50}). [d]CC_{50} assessed in HEK 293T cells. [e]CC_{50} assessed in MDCK cells. [f]Selectivity index, defined as the ratio between the CC_{50} value assessed in MDCK cells and the EC_{50} value. [g]Compound concentrations higher than those reported could not be tested in PRA due to cytotoxicity. All values represent the averages ± SD of data derived from at least three independent experiments in duplicate. ND: not determined. NC: not calculated because of cytotoxicity or absence of antiviral activity at tested concentrations.

In this model, two hydrogen bonds between the amide portion of the ligands and residues Gln408 and Val621 resemble PB1–PA interactions. When present in the ligand, a third hydrogen bond occurs between the CN nitrogen of the compound and Lys643 side chain amine. The three phenyl rings are accommodated in three hydrophobic areas indicated as I (Val621, Phe411, and Cys415), II (Pro620, Val628, and His713), and III (Phe658, Leu666, Phe707, and Phe710) in

DOI: 10.1021/acs.jmedchem.5b01935
J. Med. Chem. 2016, 59, 2688–2703

Scheme 4. Synthesis of Compound 11[a]

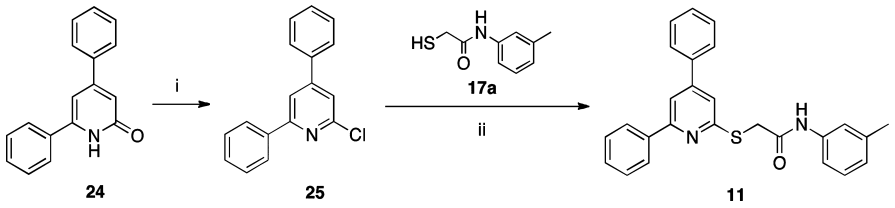

[a]Reagents and conditions: (i) $POCl_3$, reflux, 4 d; (ii) DME, CuI, L-proline, K_2CO_3, reflux in sealed ampule, 30 h.

Scheme 5. Synthesis of Compounds 2 and 9[a]

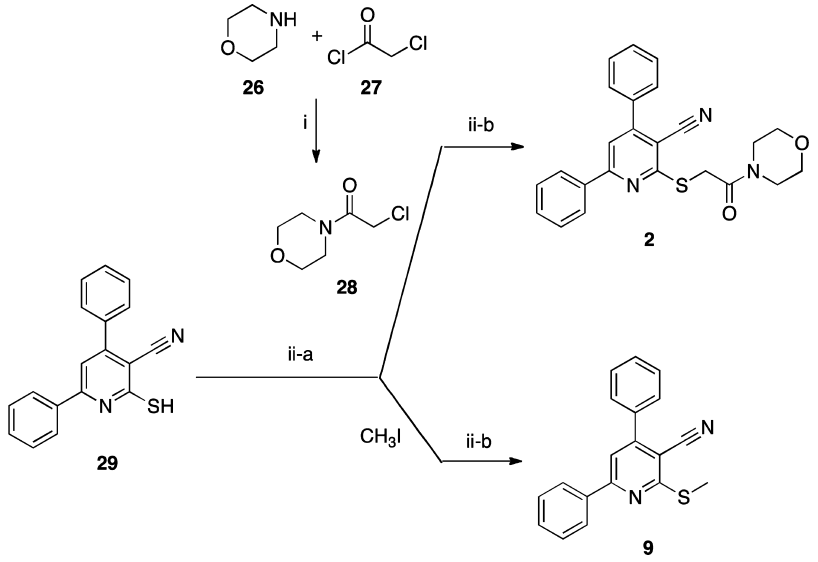

[a]Reagents and conditions: (i) K_2CO_3, THF, 0 °C to rt, 1 h; (ii-a) DMF, Cs_2CO_3, TBAI, rt, 1 h; (ii-b) 0 °C to rt, 2 h.

Table 2. Inhibitory Activity of Selected Compounds on the PA−PB1 Interaction in the Modified ELISA

compd	modified ELISA PA−PB1 interaction assay IC_{50} (μM)[a]
1	35.2 ± 5.1
4	>200
8	145 ± 24.0
11	40.5 ± 15.6
14	113 ± 15
15	64.5 ± 5.4
$PB1_{(1-15)}$-Tat peptide	31.7 ± 10.8

[a]Ability of the compounds to inhibit the PA−PB1 interaction in the ELISA performed with the DMEM serum-free medium in place of the PBS buffer. Values represent the compound concentration (in μM) that reduces the interaction between PA and PB1 by 50% (IC_{50}). Values represent the averages ± SD of data derived from at least two independent experiments in duplicate.

Table 3. Activity of the Selected Compounds in the Minireplicon Assay

compd	minireplicon assay EC_{50} (μM)[a]
1	86.6 ± 15.0
4	46.3 ± 8.7
11	30.8 ± 5.3
15	22.0 ± 4.1
RBV	23.8 ± 4.5

[a]The EC_{50} values represent the compound concentration that reduces by 50% the activity of FluA virus RNA polymerase in HEK 293T cells. All values represent the averages ± SD of data derived from at least two independent experiments in duplicate.

the figure. A further hydrophobic interaction involves Trp706 and the pyridine (or pyrimidine) ring of the small molecule.

Two examples of bad ligand placements within the binding site are shown in Figure 2, where the conformations of **12** and **3** (cyan sticks) are compared with that of compound **1** (orange sticks). As previously discussed, compounds lacking of important portions of compound **1** were not able to reproduce fundamental protein−ligand interactions in the docking simulations. In particular, the increase of IC_{50} values of molecules lacking of either one of the phenyl groups that interact with the protein regions II and III could be explained by the impossibility to form any of the important interactions, most of the time presenting a completely different binding mode, as exemplified in panel A in Figure 2. With the substitution of the sulfur atom (compounds **3**−**5**) and with the introduction of a double bond (**6**) the effective interactions were sometimes partially reproduced (exemplified in panel B in Figure 2) or completely lost. The different geometry properties of the atoms substituting the sulfur atom and of the C−C double bond do not allow the small molecule to assume a suitable conformation for correct binding, resulting in a bad docking pose and explaining the inactivity of these molecules.

Compounds **11**, **14**, and **15**, all lacking the nitrile group, were able to reproduce all the important interactions, except the hydrogen bond with Lys643, thus overlapping very well with the binding pose of **1** (Figure 3). The overlapping binding

DOI: 10.1021/acs.jmedchem.5b01935
J. Med. Chem. 2016, 59, 2688−2703

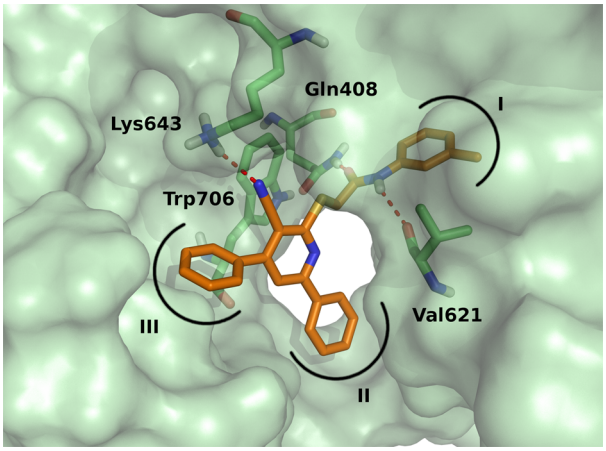

Figure 1. Binding pose for compound **1** (orange sticks).

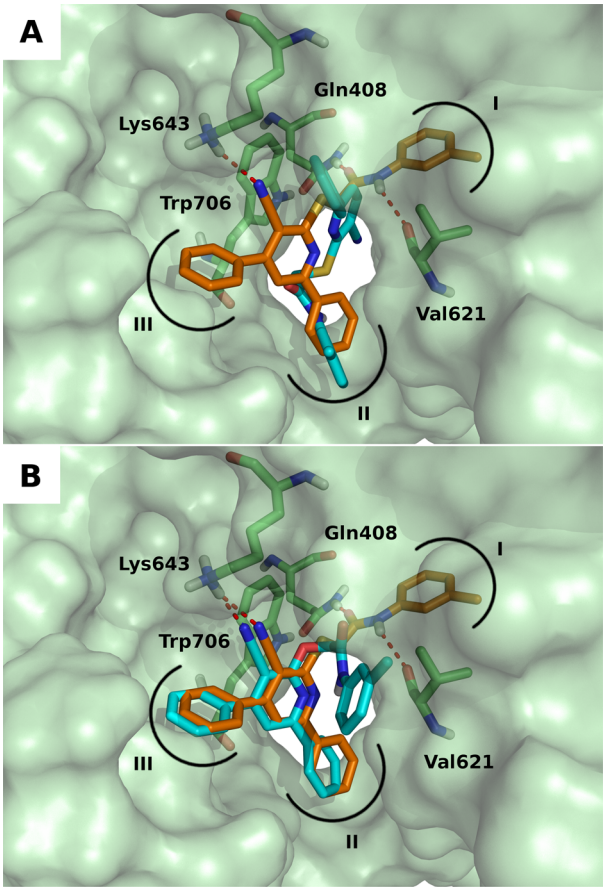

Figure 2. Examples of bad binding of inactive compounds. In both images compound **1** (orange sticks) is used as a reference. (A) Binding pose of compound **12** (cyan sticks). (B) Binding pose of compound **3** (cyan sticks).

poses of compounds **11**, **14**, and **15** can be found in Figure S1 of the Supporting Information. From the binding model, we expected that the lack of the hydrogen bond with Lys643 would result in a less favorable binding of the small molecules to PA, with a decrease in the ability to disrupt the PA−PB1 interaction, but this was not confirmed by the biological data. Thus, the PA-compound complexes for the most promising compounds (**1**, **11**, and **15**) were further investigated by means of molecular dynamics (MD) using Schrödinger Desmond.[42]

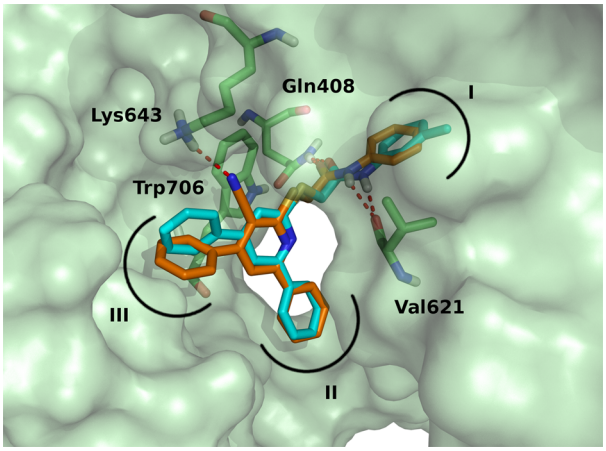

Figure 3. Binding pose of compounds **1** (orange sticks) and compound **11** (cyan sticks) from docking simulations.

After extensive equilibration, a 14 ns MD simulation was performed for each complex starting from the most representative docking pose. The evolution in time of the root-mean-square deviation (RMSD) calculated on the backbone atoms of the protein with respect to the starting structure is presented in panel A of Figure 4. After an initial increase due to further equilibration of the complex, the RMSD values were less variable in both simulations, in particular for the compound **11** in complex with PA, whose RMSD stabilized around 3.19 Å after 3 ns of simulation. For the molecular system containing compound **1** the average RMSD calculated between 2 and 8 ns was 2.61 Å, while it increased up to 3.44 Å (at 12 ns) after this time period. RMSD average values for the PA−**15** complex were 2.15 and 2.77 Å between 3 and 8 ns and after 8 ns, respectively. The root-mean-square fluctuations (RMSFs) of the backbone atoms were then evaluated on the whole trajectories. As shown in panel B of Figure 4, the RMSF trends were the same for the three systems. Predictably, high fluctuations were recorded for the protein portions (residues 349−353, 372−388, 389−396, and 550−557) that were not solved in the original crystal structure (PDB ID 2ZNL). Higher values generally corresponded to random coils and did not include residues interacting with the ligands (highlighted in purple), suggesting that the structure of PB1-binding site within PA was stable during the production MD. This was further supported by cluster analysis that indicated high similarity of the binding site conformation between the clusters. Figure 5 shows the superposition of the average structures of the ten clusters obtained for compound **1**, **11**, and **15** complexes (panels A, B, and C, respectively). In all panels, one structure of the ligand (in sticks) is shown for a better identification of the binding site.

For a more detailed analysis of the stability of the PA−ligand complexes, the interactions between the protein and the small molecules were investigated on the whole 14 ns simulation time. Occupancy percentages were also calculated and are listed in Table 4. Hydrogen bonds and ionic interactions were the most stable contacts between PA and the ligand, with occupancy higher than 60%, whereas hydrophobic interactions were generally weaker (occupancy less than 30%). An exception was the hydrophobic interaction with Trp706 that resulted to be stable and important, particularly for compound **11** (65.90% occupancy) and second for compound **15** (50.72% occupancy). Predictably, the ionic contact between Lys643 side

DOI: 10.1021/acs.jmedchem.5b01935
J. Med. Chem. 2016, 59, 2688−2703

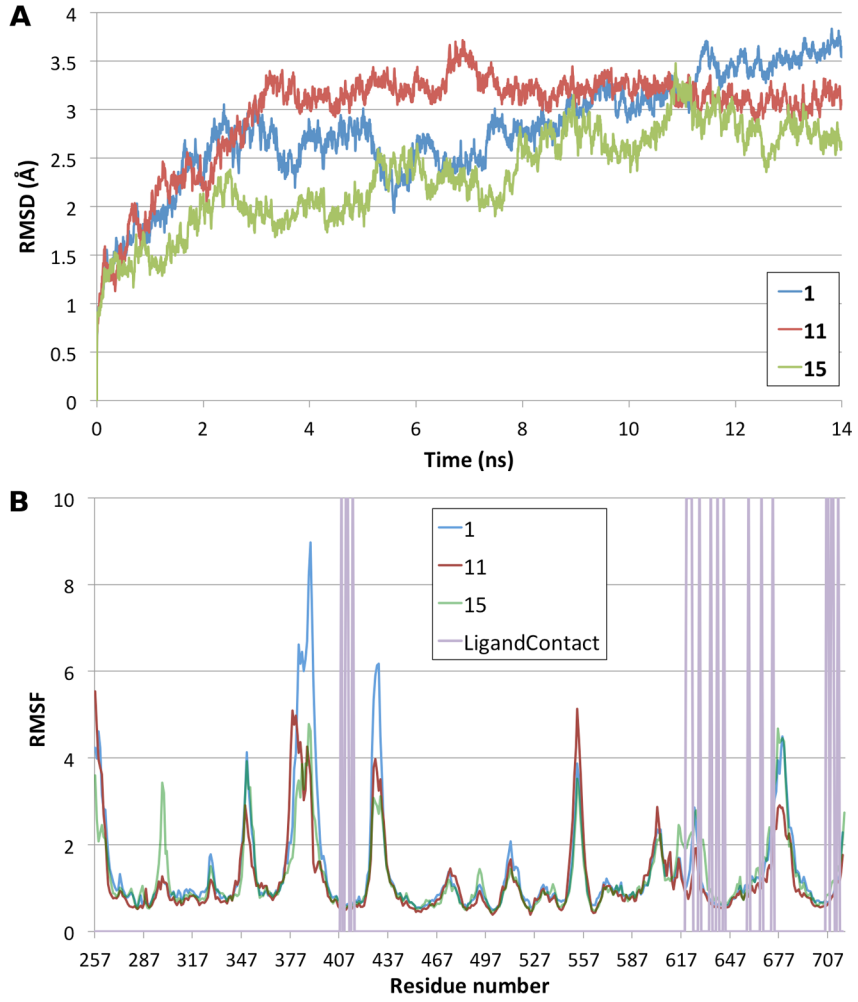

Figure 4. (A) Time evolution of the backbone atoms RMSD values for the complexes between PA and compounds **1** (blue line), **11** (red line), and **15** (green line). (B) RMSF evaluation of the backbone atoms for the complexes between PA and compounds **1** (blue line), **11** (red line), and **15** (green line). Ligand contacts are highlighted in purple.

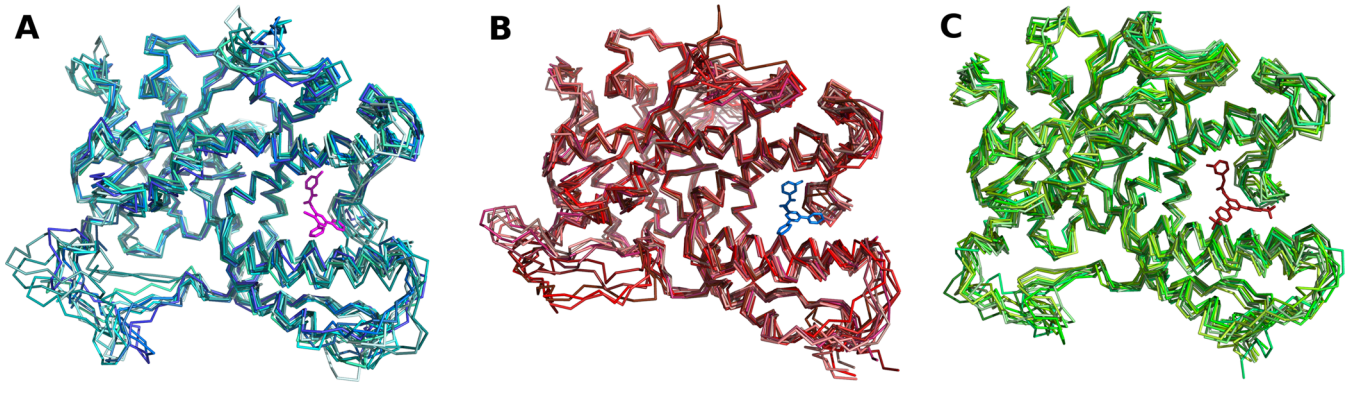

Figure 5. Superposition of the average structures of the 10 clusters obtained by cluster analysis. Protein backbone is shown as ribbon and the ligand structure in sticks. (A) Clusters for the PA–compound **1** complex. (B) Clusters for the PA–compound **11** complex. (C) Clusters for the PA–compound **15** complex.

chain amine group and the compounds was much more important in the complex between the protein and **1**, where the interaction involved the CN group of the small molecule. Differently, negligible or weak ionic contacts occurred between Lys643 and the sulfur atom of **11** and **15**, respectively. Not predicted by the docking simulation, a π–cation contact between Lys643 side chain amine and the phenyl moiety in position 4 in the pyridine core of the ligands was detected, and it appeared more stable for compound **1** (74.54% versus 31.30% occupancy for **11**). This interaction was, however, negligible for compound **15** (3.54% occupancy), where the π–cation contact was compensated by a stronger ionic interaction of Lys643 with the sulfur atom (25.88% occupancy) and by a weak hydrogen bond between Lys643 and the carbonyl oxygen

DOI: 10.1021/acs.jmedchem.5b01935
J. Med. Chem. 2016, 59, 2688–2703

Table 4. Ligand Interaction Occupancies for 1, 11, and 15 in Complex with PA

residue atom[a]	ligand atom/group	type of contact[b]	occupancy (%)[c] compd 1	compd 11	compd 15
Val621(O)	NH	bbHB	25.10	98.36	24.97
Gln408(HE)	O	scHB	22.04	97.05	14.68
Lys643(NZ)	CN or S	I	56.35	6.38	25.88
Lys643(HZ)	O	scHB	0.00	0.00	15.78
Lys643	4-phenyl	Pcat	74.54	31.30	3.54
Trp706	pyridine	Hyd	35.41	65.90	50.72
Phe411	3-Me-phenyl	Hyd	16.80	15.63	27.31
Phe411	3-Me-phenyl	PP	30.29	1.23	33.20
Cys415	3-Me-phenyl	Hyd	5.93	6.72	3.60
Pro620	6-phenyl	Hyd	4.15	0.24	0.00
Val628	6-phenyl	Hyd	3.22	0.79	3.05
Leu666	4-phenyl	Hyd	2.88	2.47	0.79
Phe707	4-phenyl	Hyd	23.69	12.61	30.02
Phe710	4-phenyl	Hyd	46.97	24.16	19.01
Phe710	4-phenyl	PP	25.77	29.66	17.75
His713	4-phenyl	PP	10.04	14.20	0.00
Lys643	N1[d]	WB	NA[d]	NA	46.09

[a]Only for hydrogen bonds and ionic contacts, the interacting atom is reported in brackets using the following abbreviations: O = backbone oxygen; HE = hydrogen of the side chain amide; NZ = nitrogen of the side chain amine; HZ = hydrogen side chain. [b]Type of interaction between the protein and the ligand. Abbreviations used: bbHB = hydrogen bond with residue backbone; scHB = hydrogen bond with residue side chain; I = ionic interaction; Pcat = π–cation interaction; Hyd = hydrophobic interaction; PP = π–π stacking; WB = water bridge. [c]Percentage of trajectory frames in which the interaction was recorded. [d]N1 = pyrimidine nitrogen in position Z in the compound, according to Table 1 numeration; NA = not applicable.

of the ligand (15.78% occupancy). Importantly, Lys643 was also involved in a water-bridge contact with the pyrimidine nitrogen in position Z (according to Table 1; henceforth named N1) of compound **15** with 46.09% occupancy, while this type of interaction is not possible for compounds **1** or **11**.

Remarkably, hydrogen bonds between the amide portion of compound **11** and Val621 backbone oxygen and Gln408 side chain amide hydrogen presented occupancy values close to 100%; while the same interactions in the other PA–compound complexes were much weaker, with occupancy lower than 30%. From the visualization of the trajectories a change of conformation of **1** and of **15** were observed. In the PA–compound **1** trajectory, while the interaction between the ligand's CN group and Lys643 occurred during the whole duration of the simulation, the hydrogen bonds with Val621 and Gln408 broke after approximately 4 ns. An approximately 1.7 Å shift of the pyridine core of **1** weakened the interaction of Trp706, placed the phenyl ring in position 4 in the pyridine in a more suitable area for the π–cation contact with Lys643, and enhanced the hydrophobic interactions with the areas II and III, explaining the higher occupancy values for these contacts (Lys643 π–cation contact and Phe707 and Phe710 hydrophobic interaction in particular). Furthermore, lacking the constraints given by the hydrogen bonds involving the ligand's amide moiety, the methyl-substituted phenyl ring was able to give weak T-shaped π–π stacking with Phe411 in the hydrophobic area I. As an example of this change in conformation, panel A of Figure 6 shows the superposition of

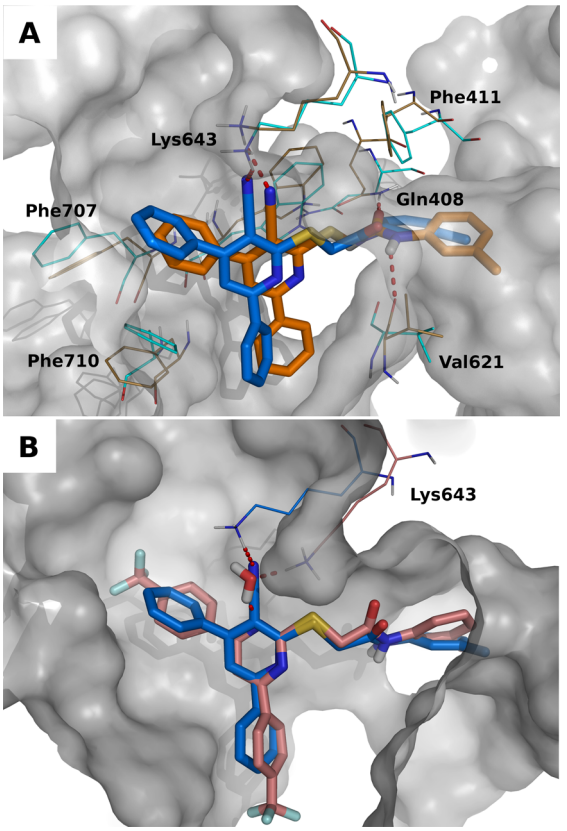

Figure 6. (A) Change in protein–ligand interactions during the MD simulation of **1** in complex with PA. The ligands and the protein residues discussed in the text are shown as sticks and as lines, respectively. Carbon atoms of the starting complex structure are colored in orange; while the ones of the saved MD trajectory frame are in light blue. Lighter shades of the same color were used for protein carbon atoms. Hydrogen bonds are indicated in red. (B) Superposition of the PA-compound **1** and PA-compound **15** complexes extracted after 4 ns of simulation. Similar representation to panel A was used here. Carbon atoms of compound **1** are colored in light blue; while the ones of compound **15** are in pink. The same color was used for protein carbon atoms. The water molecule mentioned in the text is represented in sticks.

a frame saved from the trajectory after 4.8 ns of simulation with the starting structure of the PA–compound **1** complex. Similarly to what was observed for the system containing compound **1**, after approximately 3.7 ns, a 2.3 Å shift of the central aromatic ring occurred in the PA–**15** simulation. Also in this case, the change in binding mode weakened the interaction with Trp706, increased the hydrophobic interactions with the areas II and III, with residues Phe411 and Phe707 in particular, and allowed the establishment of a weak T-shaped π–π stacking with Phe411. However, in this simulation Lys643 did not give a π–cation interaction with the phenyl moiety, but it interacted with compound **15** through a direct hydrogen bond (with the carbonyl oxygen) and a water bridge (with the pyrimidine N1 nitrogen), mainly after the compound repositioning. Interestingly, the water molecule that bridges the interaction between Lys643 and N1 overlaps very well the CN nitrogen of **1**, when the structures of the two complexes extracted after 4 ns simulation are superposed (panel B of

DOI: 10.1021/acs.jmedchem.5b01935
J. Med. Chem. 2016, 59, 2688–2703

Figure 6). Thus, in the case of **15**, the water molecule had the same role of the CN group of **1** in the interactions with the protein, and this explains why the MD simulation for the PA–**15** system was more similar to the one containing **1** than to the one containing **11**.

Taken together, the results from the MD simulations suggest that the decrease in binding affinity caused by the lack of the ionic contact between the CN group and Lys643 side chain amine is compensated by CN-lacking compounds that display an interesting activity in two possible ways according to the central scaffold. In the case of a pyrimidine central ring (**15**), N1 allows the establishment of a water bridge that mimics the CN group. For pyridine scaffolds (**11**) that do not allow this interaction a more stable binding conformation with stronger interactions with other critical residues (Val621, Gln408, and Trp706 in particular) explains the comparable activity exhibited by the two compounds.

CONCLUSIONS

The increasing resistance for the current therapy against influenza infection makes the discovery of novel drugs with a different mechanism of action compelling.[15,43] The viral RNA polymerase is not only essential for the viral genome replication and transcription but also less prone to genetic variability than the current therapeutic targets. Its activity requires the formation of the PA–PB1 complex, making the inhibition of this protein–protein interaction an attractive antiviral strategy. In this work, a hit optimization process was applied to previously identified small molecules with a 3-cyano-4,6-diphenylpyridine scaffold that were identified as promising PA–PB1 PPI.[35] The molecular scaffold was systematically modified, and synthetic strategies were developed. The biological evaluation of the 15 synthesized compounds allowed the determination of structure–activity relationships and showed for the first time that this novel class of molecules with a 4,6-diphenylpyridine (or pyrimidine) nucleus is able to inhibit the viral polymerase through the disruption of the PA–PB1 interaction and that this can result in an antiviral effect with a good toxicity profile. The biological assay results indicated that the two phenyl rings in positions 4 and 6 are essential for antiviral activity, while the removal of the CN moiety at position 3 does not affect compound activity. Furthermore, the modification of the sulfur-containing side chain produces a decrease or complete loss in the inhibition of the PA–PB1 interaction. Interestingly, some of these compounds retain some antiviral activity, indicating a possible change in the mechanism of action for them. SAR indications were rationalized by means of docking and molecular dynamics simulations that confirmed that compounds bind to the PB1-binding site within the C-terminal portion of PA and that the most important interactions involve Lys643, Gln408, Val621, Trp706, and three hydrophobic areas (I, II, and III).

Notably, three compounds (**1**, **11**, and **15**) that act on a target that is less prone to mutations than the ones exploited in current therapy were identified in this work. These are promising anti-influenza molecules that will be further developed in the future, using the binding model and the identified SAR.

EXPERIMENTAL SECTION

Computational Details. *Protein Preparation.* The homology model prepared for the previous study[35] was used as the structure for the influenza A PA–PB1 complex. Briefly, the available structures of the C-terminal portion of H1N1 and H5N5 influenza A virus PA (PAC) in complex with the N-terminal PA-binding region of PB1 (PB1N, residues 1–25) were downloaded from the Protein Data Bank (PDB ID: 2ZNL[20] and 3CM8,[21] respectively). Since both structure present gaps, a more complete PAC was obtained by means of homology modeling using the Prime tool of the Schrödinger suite.[44] The model was built of the FASTA sequence of the protein (influenza A virus, strain A/Wilson-Smith/1993 H1N1), using PDB IDs 2ZNL as the first template and 3CM8 as the second one. When possible, the missing portions of 2ZNL were thus filled using 3CM8 corresponding coordinates, while the missing residues in both structures were modeled by the program according to the FASTA sequence. In order to remove unfavorable contacts, the model was then energy minimized using the all-atom OPLS force field and Polak–Ribiere conjugate gradient method. Water was used as a solvent, applying a continuum solvation method. Convergence was set to 0.3 kJ mol^{-1}, and extended cut-offs were used.

Protein Structure Comparison. The X-ray crystal structure of the Influenza A virus H17N10 PA–PB1–PB2 trimer in complex with the viral RNA promoter was downloaded from the Protein Data Bank (PDB ID: 4WSB).[23] The C-terminal portion of PA (PAC) was used for comparison with that of the homology model. PyMOL[45] was used for structure superposition. The alignment of the residue sequences saved from the superposition was assessed with Clustal Omega web server.[46]

Ligand Preparation. All small molecules were built with the Schrödinger Maestro graphical interface.[47] The structures were then processed with Schrödinger LigPrep tool[48] generating for each ligand all feasible tautomers and assigning with Epik all possible protonation states at pH 7.0 ± 2.0, using all atom OPLS force field.

Docking Simulations. Docking simulations were performed with two programs: Glide[40] and GOLD.[41] In the docking computed with Glide, the receptor grid was built on the PA–PB1 complex and centered on the PB1 peptide derived from the crystal structure. The dimensions of the box were set to 12 Å. Default settings with flexible SP mode were chosen for the docking simulation. Generated poses were minimized after docking and a maximum of five low energy poses were saved for each entry. The docking simulations with GOLD were performed using GoldScore and ChemScore fitness functions. The search efficiency was set to 200%, and results differing less than 1.5 Å in ligand all-atom RMSD were clustered together. Also in this case five poses were saved for each entry. All poses were visually inspected, and consensus poses were used for SAR determination.

Molecular Dynamic Simulation (MD). The molecular dynamics simulations were performed on the protein–ligand complexes involving compounds **1**, **11**, and **15**. Starting structures were retrieved from the most representative docking poses results. The simulation setup was performed by means of the System Builder of Schrödinger Desmond.[42] The simulation box was orthorhombic with the minimum possible volume. A TIP4P water model and the all atom OPLS force field were used. The system was neutralized and a salt (NaCl) concentration of 0.15 M was added to the system.

The simulations were performed in PBC conditions. Prior to production, a total of 4 ns of equilibration was performed. The first step of equilibration was a 1 ns NVT Brownian simulation at 10 K temperature, restraining the solute heavy atoms. All the following steps used the Langevin algorithm. The second step of equilibration was performed restraining solute heavy atoms in NVT conditions for 0.5 ns at 10 K with Berendsen temperature coupling, using a 0.1 coupling constant. In the third stage, solute heavy atoms were restrained in NPT conditions for 0.5 ns at 10 K and 1 atm with Berendsen temperature and pressure coupling, using 0.1 and 50.0 coupling constants for temperature and pressure, respectively. Then, solute heavy atoms were restrained in NPT conditions for 1 ns at 300 K and 1 atm with Berendsen temperature and pressure coupling, using 0.1 and 2.0 coupling constants for temperature and pressure, respectively. No restraints and NPT conditions were set for the last equilibration step that lasted 1 ns at 300 K and 1 atm with Berendsen temperature and pressure coupling, using 0.1 and 2.0 coupling constants for temperature and pressure, respectively. All restraints were applied with

DOI: 10.1021/acs.jmedchem.5b01935
J. Med. Chem. 2016, 59, 2688–2703

a force of 50.0 kcal/mol. A 14 ns NPT production MD simulation was performed with a 2 fs time step, collecting energy and trajectory data every 1.2 and 4.8 ps, respectively. The temperature was maintained at 300 K, and pressure was maintained at 1 atm using Langevin method with coupling constant of 2.0 and 1.0 for pressure and temperature, respectively. The PME method with 9.0 nm cutoff radius was used for Coulombic interactions.

The MD analysis was performed with the Desmond Simulation Quality Analysis and the Simulation Interaction Diagram tools.[42] Cluster analysis was computed with the python script *trajectory_clusters.py* available in the Schrödinger suite. Ten clusters were identified, confronting all trajectory frames.

Chemistry. Chloride **16** was either bought from Advanced Chemical Intermediates Ltd. or synthesized by us through a known procedure.[49] Thiol **17a**, alcohol **17b**, and amine **17c** were obtained from Otava Ltd. Chlorides **23a** and **23b** were purchased from Fluorochem Ltd. Chloropyrimidine **23c**, pyridone **24**, and thiol **29** were prepared following literature protocols.[50−52] All other chemicals were purchased from Sigma-Aldrich. THF, toluene, DME, and DCM were distilled freshly from CaH_2, all other solvents were used as received. Unless indicated otherwise, all reactions were carried out under an inert atmosphere. TLC analyses were performed with Merck F254 Alumina Silica Plates using UV visualization or staining. Microwave reactions were carried out on a Biotage Initiator. Column purifications were carried out manually using Silicycle Ultra Pure Silica Gel, Fluka silica gel 60 (0.04−0.063 mm), or automatically using the Biotage equipment. All HRMS spectra were recorded on Bruker micrOTOF MS using ESI in positive ion mode. The ^{1}H-, ^{13}C-, and 2D-NMR spectra were recorded on a Bruker 200, 250, 400, 500, or 600 MHz spectrometer. Systematic names for molecules were generated using ChemBioDraw Ultra 14. Unless specified otherwise, all final compounds have an LC purity ≥95% at 254 nm. This was determined using a Shimadzu HPLC/MS workstation with a LC-20AD pump system, SPD-M20A diode array detection, and a LCMS-2010 EV Liquid Chromatograph Mass Spectrometer. Compound purities were calculated as the percentage peak area of the analyzed compound by UV detection at 254 nm. The buffer used is a 0.4% (w/v) NH_4HCO_3 solution in water, adjusted to pH 8.0 with NH_4OH. The column used is an Xbridge C18 5 μm column (50 mm × 4.6 mm). Solvents used in this paragraph: Solvent B = 90% MeCN/10% buffer; Solvent A = 90% water/10% buffer. The analysis was conducted using a flow rate of 1.0 mL/min, start 5% B, linear gradient to 90% B in 4.5 min, then 1.5 min at 90% B, then linear gradient to 5% in 0.5 min, then 1.5 min at 5% B, total run time of 8 min.

*2-((3-Cyano-4,6-diphenylpyridin-2-yl)thio)-N-(m-tolyl)acetamide (**1**, VUF14465).* To a stirred solution of chloride **16** (0.291 g, 1.00 mmol) in DMF (20 mL) was added thiol **17a** (0.326 g, 1.80 mmol) and K_2CO_3 (0.207 g, 1.50 mmol). The resulting mixture was stirred for 1 h and then quenched with water (50 mL). The precipitate was filtered and dissolved in DCM. The solution was dried over Na_2SO_4, filtered, and concentrated. The crude product was purified using flash chromatography (gradient starting from 5% (1% Et_3N/EtOAc) in heptane to 40% (1% Et_3N/EtOAc) in heptane). This yielded the product as a solid (110 mg, 25%). ^{1}H NMR (500 MHz, $CDCl_3$) δ 9.02 (s, 1H), 8.14−8.03 (m, 2H), 7.68−7.60 (m, 3H), 7.60−7.51 (m, 6H), 7.12−7.00 (m, 2H), 6.81 (s, 2H), 4.14 (s, 2H), 2.15 (s, 3H). ^{13}C NMR (126 MHz, $CDCl_3$) δ 166.5, 162.6, 159.6, 155.5, 138.8, 137.7, 137.2, 135.8, 131.3, 130.6, 129.6, 129.4, 128.9, 128.5, 127.7, 125.1, 120.3, 117.4, 116.7, 115.2, 104.3, 35.2, 21.5. LCMS purity: 98+ %. HRMS $[M + H]^+$ calc, 436.1478; found, 436.1467.

*2-((2-Morpholino-2-oxoethyl)thio)-4,6-diphenylnicotinonitrile (**2**, BAS-88).* A mixture of thiol **29** (173 mg, 0.600 mmol), Cs_2CO_3 (195 mg, 0.599 mmol), TBAI (222 mg, 0.601 mmol), and anhydrous DMF (8 mL) was stirred for 1 h at rt. After cooling to 0 °C, chloride **28** (147 mg, 0.899 mmol) dissolved in DMF (0.4 mL) was added. The resulting mixture was allowed to warm to rt and stirred for 2 h. After dilution with cold water (30 mL) and extraction with DCM (3 × 20 mL), the combined organic layers were dried over $MgSO_4$, filtered, and concentrated. The residue was purified by column chromatography (acetone/DCM 5/95) to obtain the product as white solid (75 mg, 30%). ^{1}H NMR (600 MHz, $CDCl_3$) δ 8.05−8.01 (m, 2H), 7.64−7.60 (m, 2H), 7.59−7.50 (m, 7H), 4.31 (s, 2H), 3.74−3.66 (m, 8H). ^{13}C NMR (150.92 MHz, $CDCl_3$) δ 166.2, 162.2, 158.8, 154.8, 137.4, 136.0, 130.7, 130.2, 129.1, 129.0, 128.4, 127.4, 116.5, 115.4, 103.8, 66.8, 66.6, 46.6, 42.7, 32.9. LCMS purity: 95+ %. HRMS $[M + H]^+$ calc, 416.1427; found, 416.1434.

*2-((3-Cyano-4,6-diphenylpyridin-2-yl)oxy)-N-(m-tolyl)acetamide (**3**, VUF14467).* A microwave tube was charged with chloride **16** (0.15 g, 0.52 mmol), alcohol **17b** (0.077 g, 0.47 mmol), CuI (8.9 mg, 0.047 mmol), and Cs_2CO_3 (0.229 g, 0.704 mmol). The tube was thoroughly flushed with N_2. MeCN (5 mL) was added, and the mixture was exposed to μW radiation (120 °C, 1.5 h). The reaction mixture was concentrated under reduced pressure. The remaining solids were subjected to extraction with EtOAc/water (3 × 50 mL). The organic layer was dried over $MgSO_4$, filtered, and concentrated. The crude product was purified by column chromatography using EtOAc/heptane 2:8 and then (EtOAc/Et_3N 99:1)/heptane 25:75. This afforded the product as a solid (14 mg, 6%). ^{1}H NMR (500 MHz, DMSO-d_6) δ 10.35 (s, 1H), 8.23−8.15 (m, 2H), 7.87 (s, 1H), 7.80−7.74 (m, 2H), 7.64−7.58 (m, 3H), 7.48−7.45 (m, 2H), 7.40−7.37 (m, 3H), 7.21 (t, *J* = 7.8 Hz, 1H), 6.89 (d, *J* = 7.5 Hz, 1H), 5.17 (s, 2H), 2.27 (s, 3H). ^{13}C NMR (126 MHz, DMSO-d_6) δ 166.1, 163.3, 157.0, 156.6, 138.5, 138.0, 136.3, 135.8, 130.8, 130.2, 128.9, 128.8, 128.7, 127.5, 124.2, 120.0, 116.6, 115.2, 114.2, 92.3, 65.7, 21.2, two carbon signals likely overlap. LCMS purity: 95+ %. HRMS $[M + H]^+$ calc, 420.1707; found, 420.1702.

*2-((3-Cyano-4,6-diphenylpyridin-2-yl)amino)-N-(m-tolyl)-acetamide (**4**, VUF14466).* To a stirred solution of chloride **16** (0.210 g, 0.722 mmol) in DMF (20 mL) was added amine **17c** (0.214 g, 1.30 mmol) and K_2CO_3 (0.150 g, 1.09 mmol). The resulting mixture was stirred for 18 h at 45 °C and then quenched with water (50 mL). Water and DMF were evaporated, and the residue was dissolved in DCM. This solution was dried (Na_2SO_4), filtered, and concentrated. The crude product was purified using flash chromatography (gradient starting from 10% (1% Et_3N/EtOAc) in heptane to 80% (1% Et_3N/EtOAc) in heptane). The product was collected and again subjected to the same purification procedure. This yielded the product as a solid (14 mg, 5%). ^{1}H NMR (500 MHz, $CDCl_3$) δ 8.48 (s, 1H), 8.06−8.04 (m, 2H), 7.68−7.60 (m, 2H), 7.58−7.50 (m, 3H), 7.48−7.46 (m, 3H), 7.29 (s, 1H), 7.23 (d, *J* = 8.0 Hz, 1H), 7.19 (s, 1H), 7.14 (t, *J* = 7.8 Hz, 1H), 6.88 (d, *J* = 7.4 Hz, 1H), 6.06 (t, *J* = 5.5 Hz, 1H), 4.40 (d, *J* = 5.6 Hz, 2H), 2.25 (s, 3H). ^{13}C NMR (126 MHz, $CDCl_3$) δ 168.1, 159.1, 158.8, 155.7, 139.0, 137.6, 137.5, 136.8, 130.7, 130.2, 129.2, 129.1, 129.0, 128.3, 127.5, 125.3, 120.7, 117.1, 116.9, 111.4, 89.9, 47.4, 21.5. LCMS purity: 99+ %. HRMS $[M + H]^+$ calc, 419.1866; found, 419.1861.

*3-(3-Cyano-4,6-diphenylpyridin-2-yl)-N-(m-tolyl)propanamide (**5**, VUF14519).* A mixture of **6** (63 mg, 0.15 mmol) and 5% Pd/C (5 mg, 0.05 mmol) in EtOAc (20 mL) was stirred under H_2 atmosphere (1 bar) at rt. After 6 h, more Pd/C (1 mg) was added, and hydrogenation was continued for 5 h. The black suspension was filtered over Hyflo. The filtrate was concentrated to obtain the product (44 mg, 67%). ^{1}H NMR (500 MHz, $CDCl_3$) δ 8.12 (br s, 1H), 8.03 (d, *J* = 7.7 Hz, 2H), 7.71 (s, 1H), 7.68−7.59 (m, 2H), 7.59−7.51 (m, 3H), 7.51−7.46 (m, 1H), 7.43 (t, *J* = 7.4 Hz, 2H), 7.22 (d, *J* = 8.0 Hz, 1H), 7.19−7.08 (m, 2H), 6.87 (d, *J* = 7.4 Hz, 1H), 3.67 (t, *J* = 6.3 Hz, 2H), 3.06 (t, *J* = 6.3 Hz, 2H), 2.24 (s, 3H). ^{13}C NMR (126 MHz, $CDCl_3$) δ 170.6, 163.9, 159.2, 154.6, 138.9, 138.2, 137.8, 136.4, 130.7, 130.2, 129.2, 128.9, 128.6, 127.8, 124.9, 120.3, 118.8, 116.7, 116.6, 106.2, 34.7, 32.0, 21.6, two carbon signals likely overlap. LCMS purity 95%. HRMS $[M + H]^+$ calc, 418.1914; found, 418.1909.

*(E)-3-(3-Cyano-4,6-diphenylpyridin-2-yl)-N-(m-tolyl)acrylamide (**6**, VUF14518).* A mixture consisting of chloride **16** (192 mg, 0.66 mmol), acrylamide **18** (160 mg, 0.99 mmol), NaOAc (65 mg, 0.79 mmol), nBu_4NBr (234 mg, 0.73 mmol), (*o*-Tol)$_3$P (40 mg, 0.13 mmol), and $Pd(OAc)_2$ (17 mg, 0.08 mmol) in DMF (20 mL) was stirred for 18 h at 145 °C. The green/brown suspension was diluted with satd. aq. $NaHCO_3$ soln. The mixture was extracted with EtOAc (2 × 20 mL). The combined organic layers were washed with water (3 × 20 mL) and brine (1 × 20 mL). The organic layer was dried

DOI: 10.1021/acs.jmedchem.5b01935
J. Med. Chem. 2016, 59, 2688−2703

($MgSO_4$), filtered, and concentrated. The residue was purified by column chromatography (25% EtOAc in heptane) to give the product (173 mg, 63%). ^{1}H NMR (500 MHz, CD_3OD) δ 8.36−8.29 (m, 2H), 8.17 (d, J = 14.8 Hz, 1H), 8.05 (s, 1H), 7.85 (d, J = 14.8 Hz, 1H), 7.77−7.71 (m, 2H), 7.63−7.49 (m, 8H), 7.24 (t, J = 7.8 Hz, 1H), 6.98 (d, J = 7.5 Hz, 1H), 2.36 (s, 3H). ^{13}C NMR (126 MHz, CD_3OD) δ 165.3, 160.8, 157.1, 156.1, 140.0, 139.8, 138.7, 137.8, 136.6, 131.9, 131.8, 131.2, 130.1, 130.1, 129.8, 129.8, 128.8, 126.4, 121.8, 121.5, 118.5, 117.1, 107.6, 21.6. LCMS purity 98+ %. HRMS $[M + H]^+$ calc, 416.1763; found, 416.1762.

*3-((3-Cyano-4,6-diphenylpyridin-2-yl)thio)-N-(m-tolyl)-propanamide (**7**, VUF14520).* To a stirred solution of thiol **17d** (200 mg, 1.02 mmol) in MeCN (10 mL) at 0 °C were added chloride **16** (298 mg, 1.02 mmol) and K_2CO_3 (142 mg, 1.02 mmol). The resulting mixture was stirred for 0.5 h at 0 °C and then 3 h at rt. The mixture was concentrated under reduced pressure and purified by flash chromatography (gradient starting from 5% (1% Et_3N/EtOAc) in heptane to 80% (1% Et_3N/EtOAc) in heptane). This afforded the product (160 mg, 35%). ^{1}H NMR (400 MHz, $CDCl_3$) δ 8.11 (dd, J = 6.4, 2.7 Hz, 2H), 7.66−7.58 (m, 2H), 7.58−7.44 (m, 7H), 7.31 (s, 1H), 7.24−7.11 (m, 3H), 6.92 (d, J = 7.2 Hz, 1H), 3.79 (t, J = 7.2 Hz, 2H), 2.91 (t, J = 7.2 Hz, 2H), 2.31 (s, 3H). ^{13}C NMR (101 MHz, $CDCl_3$) δ 169.1, 163.5, 158.9, 154.9, 139.1, 137.7, 137.5, 136.3, 130.9, 130.3, 129.3, 129.2, 129.0, 128.5, 127.5, 125.4, 120.7, 117.1, 116.2, 115.7, 104.3, 37.7, 26.5, 21.6. LCMS purity: 98+ %. HRMS $[M + H]^+$ calc, 450.1635; found, 450.1638.

*4-((3-Cyano-4,6-diphenylpyridin-2-yl)thio)-N-(m-tolyl)-butanamide (**8**, VUF14523).* To a stirred solution of thiol **17e** (120 mg, 0.573 mmol) in MeCN (10 mL) at 0 °C were added chloride **16** (167 mg, 0.573 mmol) and K_2CO_3 (79 mg, 0.57 mmol). The resulting mixture was stirred for 0.5 h at 0 °C and 3 h at rt. The resulting mixture was concentrated under reduced pressure and purified by flash chromatography (gradient starting from 5% (1% Et_3N/EtOAc) in heptane to 80% (1% Et_3N/EtOAc) in heptane). This afforded the product (20 mg, 8%). ^{1}H NMR (400 MHz, $CDCl_3$) δ 8.13−8.04 (m, 2H), 7.65−7.59 (m, 2H), 7.55−7.51 (m, 4H), 7.50−7.46 (m, 3H), 7.36 (s, 1H), 7.26−7.12 (m, 3H), 6.90 (d, J = 7.2 Hz, 1H), 3.55 (t, J = 6.5 Hz, 2H), 2.59 (t, J = 7.1 Hz, 2H), 2.38−2.25 (m, 5H). ^{13}C NMR (101 MHz, $CDCl_3$) δ 170.2, 163.5, 158.7, 154.6, 138.9, 137.7, 137.3, 136.2, 130.6, 130.1, 129.1, 129.0, 128.8, 128.4, 127.4, 125.1, 120.4, 116.8, 115.9, 115.9, 103.9, 36.0, 30.0, 24.8, 21.5. LCMS purity: 95+ %. HRMS $[M + H]^+$ calc, 464.1791; found, 464.1785.

*2-(Methylthio)-4,6-diphenylnicotinonitrile (**9**, BAS-85).* To a stirred solution of thiol **29** (144 mg, 0.499 mmol) in anhydrous DMF (6 mL) were added Cs_2CO_3 (163 mg, 0.500 mmol) and TBAI (185 mg, 0.501 mmol). The resulting mixture was stirred for 1 h at rt. After cooling to 0 °C, MeI (0.106 g, 0.75 mmol) dissolved in DMF (0.3 mL) was introduced via syringe. The mixture was warmed to rt and stirred for an additional 2 h. After quenching with cold water (20 mL), the mixture was extracted with DCM (3 × 15 mL). The combined organic layers were dried over $MgSO_4$, filtered, and the solvents removed under vacuum. The residue was purified by column chromatography (*n*-hexane/Et_2O 5:1) yielding the product as a white solid (51 mg, 34%). ^{1}H NMR (600 MHz, $CDCl_3$) δ 8.14−8.12 (m, 2H), 7.64−7.63 (m, 2H), 7.55−7.51 (m, 7H), 2.79 (s, 3H). ^{13}C NMR (150.92 MHz, $CDCl_3$) δ 164.5, 158.4, 154.3, 137.5, 136.3, 130.6, 130.0, 129.0, 129.0, 128.4, 127.4, 115.9, 115.5, 103.7, 13.7. LCMS purity: 97+ %. HRMS $[M + H]^+$ calc, 303.0950; found, 303.0939.

*4,6-Diphenylnicotinonitrile (**10**, BAS-87).* $PdCl_2$ (2.5 mg, 0.014 mmol) was added to a degassed suspension of chloride **16** (290 mg, 1.00 mmol) and NaOAc (165 mg, 2.01 mmol) in MeOH (8 mL). The heterogeneous mixture was stirred under hydrogen (1 atm) at rt. After 36 h, the suspension was filtered and the precipitate was carefully washed with methanol (2 × 5 mL) and DCM (3 × 10 mL). The combined organic filtrates were evaporated under reduced pressure, and DCM (20 mL) was added to the residue. The resulting solution was filtered through a thin pad of silica gel, which was washed with an additional portion of DCM. After removal of the solvent under reduced pressure, the crude product was purified by column chromatography (*n*-hexane/Et_2O 4:1), affording the target compound as white solid (97 mg, 38%). ^{1}H NMR (600 MHz, $CDCl_3$) δ 9.01 (s, 1H), 8.10−8.08 (m, 2H), 7.88 (s, 1H), 7.69−7.67 (m, 2H,), 7.59−7.50 (m, 6H). ^{13}C NMR (150.92 MHz, $CDCl_3$) δ 160.5, 154.0, 153.0, 137.5, 135.9, 130.6, 130.2, 129.2, 129.1, 128.4, 127.5, 120.4, 117.2, 106.6. LCMS purity: 99+ %. HRMS $[M + H]^+$ calc, 257.1073; found, 257.1073.

*2-((4,6-Diphenylpyridin-2-yl)thio)-N-(m-tolyl)acetamide (**11**, BAS-86).* A glass tube was charged with chloride **25** (200 mg, 0.75 mmol), CuI (15 mg, 0.079 mmol), L-proline (20 mg, 0.17 mmol), and K_2CO_3 (210 mg, 1.5 mmol). The tube was evacuated and filled with argon (3 cycles). Thiol **17a** (0.150 g, 0.825 mmol) dissolved in anhydrous DME (2 mL) was introduced via syringe. The tube was sealed and heated under reflux for 30 h while stirring. After cooling to rt, the reaction mixture was partitioned between DCM (20 mL) and satd. aq. NaCl (10 mL). The organic layer was separated, and the aqueous layer was extracted with DCM (2 × 10 mL). The combined organic layers were dried over $MgSO_4$, filtered, and the solvent removed under reduced pressure. The crude product was purified by column chromatography (DCM/MeOH 6:0.1), affording the target compound as white solid (65 mg, 21%). ^{1}H NMR (600 MHz, $CDCl_3$) δ 9.97 (br s, 1H, NH), 8.08−8.04 (m, 2H), 7.71 (d, 1H, J = 1.4 Hz), 7.68−7.64 (m, 2H), 7.55−7.48 (m, 6H), 7.44 (d, 1H, J = 1.4 Hz), 7.07−6.95 (m, 2H), 6.74 (d, 1H, J = 7 Hz), 6.62 (s, 1H), 4.05 (s, 2H), 2.07 (s, 3H). ^{13}C NMR (150.92 MHz, $CDCl_3$) δ 168.1, 158.2, 158.0, 150.6, 138.7, 138.4, 138.2, 137.6, 129.8, 129.6, 129.3, 129.2, 128.6, 127.2, 127.2, 124.4, 119.9, 118.6, 116.4, 116.1, 35.1, 21.1. LCMS purity: 99+ %. HRMS $[M + H]^+$ calc, 411.1526; found, 411.1529.

*2-((3-Cyano-6-phenylpyridin-2-yl)thio)-N-(m-tolyl)acetamide (**12**, VUF14469).* To a stirred solution of chloride **23a** (0.100 g, 0.466 mmol) in MeCN (10 mL) at 0 °C in the dark were added thiol **17a** (0.093 g, 0.51 mmol) and K_2CO_3 (0.097 g, 0.70 mmol). The resulting mixture was stirred for 0.5 h at rt and then concentrated. The crude product was purified by column chromatography (using a gradient starting from 15% (1% Et_3N/EtOAc) in heptane to 80% (1% Et_3N/EtOAc) in heptane). This provided the product as a solid (17 mg, 10%). *Note*: All of this work, including the column chromatography, has to be done in the dark as the compound is photolytically unstable (as proven by NMR and LCMS studies after exposing the compound to day light). ^{1}H NMR (500 MHz, $CDCl_3$) δ 7.67 (s, 1H), 7.58−7.45 (m, 3H), 7.35 (s, 1H), 7.31 (d, J = 7.2 Hz, 2H), 7.28−7.20 (m, 3H), 6.98 (d, J = 7.3 Hz, 1H), 6.81 (d, J = 11.9 Hz, 1H), 3.73 (s, 2H), 2.35 (s, 3H). ^{13}C NMR (126 MHz, $CDCl_3$) δ 163.7, 163.6, 155.2, 139.4, 136.9, 134.2, 131.49, 129.5, 129.4, 129.2, 126.2, 120.9, 118.8, 117.3, 114.1, 112.2, 80.2, 37.9, 21.6. LCMS purity: 95+ %. HRMS $[M + H]^+$ calc, 360.1165; found, 360.1166.

*2-((3-Cyano-4-phenylpyridin-2-yl)thio)-N-(m-tolyl)acetamide (**13**, VUF14468).* To a stirred mixture of chloride **23b** (100 mg, 0.466 mmol) and NaOAc (57.3 mg, 0.699 mmol) in MeCN (5 mL) was added thiol **17a** (84 mg, 0.46 mmol). The mixture was stirred overnight at rt after which the temperature was raised to 40 °C. After 5 d, the solvent was evaporated and the remaining solids were subjected to extraction with DCM (40 mL) and water (2 × 20 mL) then brine (20 mL). The organic layer was dried ($MgSO_4$), filtered, and concentrated. The crude product was purified by column chromatography (using a gradient from 1:9 EtOAc/heptane to 5:5 EtOAc/heptane). This yielded the product as a solid (25 mg, 15%). ^{1}H NMR (400 MHz, $CDCl_3$) δ 9.03 (br, 1H), 8.67 (d, J = 5.2 Hz, 1H), 7.63−7.50 (m, 5H), 7.36 (s, 1H), 7.27−7.24 (m, 2H), 7.19 (t, J = 7.8 Hz, 1H), 6.92 (d, J = 7.4 Hz, 1H), 4.05 (s, 2H), 2.34 (s, 3H). ^{13}C NMR (101 MHz, $CDCl_3$) δ 166.5, 162.9, 154.8, 151.3, 139.2, 137.8, 135.3, 130.7, 129.4, 129.0, 128.6, 125.4, 120.8, 120.5, 116.9, 114.8, 106.5, 35.2, 21.7. LCMS purity: 98+ %. HRMS $[M + H]^+$ calc, 360.1165; found, 360.1167.

*2-((4,6-Diphenylpyrimidin-2-yl)thio)-N-(m-tolyl)acetamide (**14**, VUF14477).* To a stirred solution of chloride **23c** (150 mg, 0.562 mmol) in MeCN (10 mL) at 0 °C were added thiol **17a** (112 mg, 0.619 mmol) and K_2CO_3 (117 mg, 0.844 mmol). The resulting mixture was stirred for 5 h while being allowed to warm to rt. The solvent was partially evaporated, and the resulting mixture was filtered. The residue was dissolved in EtOAc and subjected to column

DOI: 10.1021/acs.jmedchem.5b01935
J. Med. Chem. 2016, 59, 2688−2703

chromatography (100% EtOAc). This yielded the product as a solid (120 mg, 52% yield). ^{1}H NMR (500 MHz, $CDCl_3$) δ 9.28 (s, 1H), 8.14−8.06 (m, 4H), 7.81 (s, 1H), 7.56−7.46 (m, 6H), 7.05 (d, J = 8.3 Hz, 1H), 6.98 (t, J = 7.8 Hz, 1H), 6.78 (s, 1H), 6.73 (d, J = 7.4 Hz, 1H), 4.00 (s, 2H), 2.07 (s, 3H). ^{13}C NMR (126 MHz, $CDCl_3$) δ 171.1, 167.4 (split), 165.6, 138.6, 137.9 (split), 136.3, 131.6, 129.2, 128.7, 127.4, 124.8 (split), 120.1 (split), 116.5 (split), 109.2, 35.9 (split), 21.3, splitting of some peaks was observed. LCMS purity: 99+ %. HRMS $[M + H]^+$ calc, 412.1484; found, 412.1489.

*2-((4,6-Bis(4-trifluoromethyl)phenyl)pyrimidin-2-yl)thio)-N-(m-tolyl)acetamide (**15**, VUF14525).* Thiol **17a** (54 mg, 0.30 mmol) and K_2CO_3 (21 mg, 0.15 mmol) were added to a stirred solution of chloride **23d** (40 mg, 0.099 mmol) in MeCN (10 mL) at 0 °C. The mixture was stirred for 2.5 h while being allowed to warm to rt. The solvent was partially evaporated, and the resulting mixture was filtered. The residue was purified by column chromatography (heptane/EtOAc 4:1) to yield the compound as a white solid (20 mg, 37%). ^{1}H NMR (400 MHz, $CDCl_3$) δ 8.79 (br s, 1H), 8.26 (d, J = 8.2 Hz, 4H), 7.89 (s, 1H), 7.81 (d, J = 8.3 Hz, 4H), 7.18 (d, J = 8.2 Hz, 1H), 7.09 (t, J = 7.8 Hz, 1H), 6.99 (s, 1H), 6.84 (d, J = 7.5 Hz, 1H), 4.05 (s, 2H), 2.18 (s, 3H). ^{13}C NMR (101 MHz, $CDCl_3$) δ 171.4, 166.6, 164.5, 139.3, 138.9, 137.5, 133.3 (q, ^2J = 32.8 Hz), 128.9, 127.9, 126.2 (q, ^3J = 3.8 Hz), 125.2, 123.7 (q, ^1J = 272.5 Hz), 120.2, 116.6, 109.6, 36.0, 21.3. LCMS purity: 95%. HRMS $[M + H]^+$ calc, 548.1226; found, 548.1216.

*3-Mercapto-N-(m-tolyl)propanamide (**17d**).* 3-Mercaptopropanoic acid (1.06 g, 10.0 mmol) was combined with *m*-toluidine (1.093 mL, 10.0 mmol). After 1 h of stirring at rt, the mixture was heated in the microwave for 1 h at 180 °C. The crude product was purified using column chromatography (25% EtOAc in heptane). This afforded the product (1.64 g, 84%). ^{1}H NMR (250 MHz, $CDCl_3$) δ 7.39 (s, 1H), 7.32 (br s, 1H), 7.28 (d, J = 8.1 Hz, 1H), 7.20 (t, J = 7.8 Hz, 1H), 6.94 (d, J = 7.5 Hz, 1H), 2.93−2.85 (m, 2H), 2.67 (t, J = 6.6 Hz, 2H), 2.33 (s, 3H), 1.70 (t, J = 8.5 Hz, 1H). ^{13}C NMR (126 MHz, $CDCl_3$) δ 169.2, 139.3, 137.7, 129.1, 125.6, 120.8, 117.2, 41.6, 21.7, 20.6. LCMS purity: 95+ %.

*4-Mercapto-N-(m-tolyl)butanamide (**17e**).* Dihydrothiophen-2(3*H*)-one (0.866 mL, 10.0 mmol) was mixed with *m*-toluidine (1.09 mL, 10.0 mmol) at −5 °C. The mixture was heated in the microwave (3 h at 120 °C, then 1 h at 160 °C, and finally 24 h at 180 °C), resulting in partial conversion. The mixture was purified using column chromatography (25% EtOAc in heptane). This afforded the product (375 mg, 18%). ^{1}H NMR (500 MHz, $CDCl_3$) δ 7.38 (s, 1H), 7.29−7.26 (m, 1H), 7.20 (t, J = 7.8 Hz, 1H), 7.16 (br s, 1H), 6.93 (d, J = 7.4 Hz, 1H), 2.70−2.60 (m, 2H), 2.51 (t, J = 7.2 Hz, 2H), 2.34 (s, 3H), 2.04 (p, J = 7.0 Hz, 2H), 1.36 (t, J = 8.0 Hz, 1H). ^{13}C NMR (126 MHz, $CDCl_3$) δ 170.4, 139.2, 137.8, 129.0, 125.3, 120.6, 117.0, 35.8, 29.3, 24.2, 21.6. LCMS purity: 95+ %.

*N-(m-Tolyl)acrylamide (**18**).* Acryloyl chloride (0.41 mL, 5.3 mmol) was added to a stirred solution of *m*-toluidine (0.54 mL, 5.0 mmol) and Et_3N (0.89 mL, 6.4 mmol) in THF (10 mL) at 0 °C. The orange suspension was stirred for 2.5 h and poured onto brine (10 mL). The mixture was extracted with *t*BuOMe (2×). The organic layers were dried over Na_2SO_4, filtered, and concentrated. The crude product was purified by column chromatography (25% EtOAc in heptane) to obtain the product as a transparent oil (0.57 g, 70%). ^{1}H NMR (250 MHz, $CDCl_3$) δ 7.45 (s, 1H), 7.38−7.29 (m, 1H), 7.30 (br, 1H), 7.20 (t, J = 7.9 Hz, 1H), 6.95 (d, J = 7.4 Hz, 1H), 6.43 (dd, J = 16.8, 1.3 Hz, 1H), 6.24 (dd, J = 16.8, 10.1 Hz, 1H), 5.76 (dd, J = 10.0, 1.4 Hz, 1H), 2.34 (s, 3H). LCMS purity: 97%.

*2-Chloro-4,6-diphenylpyrimidine (**23c**).* Prepared according to a published procedure.[50] ^{1}H NMR (500 MHz, $CDCl_3$) δ 8.19−8.12 (m, 4H), 8.02 (s, 1H), 7.59−7.48 (m, 6H).^{13}C NMR (126 MHz, $CDCl_3$) δ 167.7, 162.1, 135.7, 131.7, 129.1, 127.5, 111.0. LCMS purity: 95+ %.

*2-Chloro-4,6-bis(4-(trifluoromethyl)phenyl)pyrimidine (**23d**).* 2,4,6-Trichloropyrimidine (92 mg, 0.50 mmol), 4-(trifluoromethyl)-phenylboronic acid (190 mg, 1.00 mmol), and K_2CO_3 (428 mg, 3.10 mmol, dissolved in a minimum amount of H_2O) were mixed with 1,2-dimethoxyethane (10 mL). The flask was covered with aluminum foil. $Pd(OAc)_2$ (3 mg, 0.01 mmol) and PPh_3 (7 mg, 0.03 mmol) were added to the mixture. The mixture was heated at 60 °C for 24 h. The solvent was removed by rotary evaporation, and the residue subjected to extraction with DCM and H_2O. The organic layer was washed three times with H_2O, dried over Na_2SO_4, filtered, and concentrated. The residue was purified by three successive column chromatography operations (heptane/EtOAc 6:1, then PhMe/MeCOMe 8:1, and PhMe/heptane 4:1). This yielded the product as a clear oil, which slowly crystallized (40 mg, 20%). ^{1}H NMR (250 MHz, $CDCl_3$) δ 8.28 (d, J = 8.1 Hz, 4H), 8.08 (s, 1H), 7.82 (d, J = 8.3 Hz, 4H). LCMS purity: 95%.

*2-Chloro-4,6-diphenylpyridine (**25**).* A mixture of pyridone **24** (370 mg, 1.50 mmol) and $POCl_3$ (3.0 mL) was heated under reflux for 4 d. After cooling to rt the crude product was poured onto crushed ice. The mixture was neutralized with cold 15% aq. KOH, and the precipitate was collected by filtration, washed with water, and dissolved in DCM. The resulting solution was washed once more with diluted KOH and water. After drying the organic layer over $MgSO_4$ and filtration, the solvent was removed under reduced pressure. The crude product was purified by column chromatography (DCM) yielding the target compound as white solid (213 mg, 53%). ^{1}H NMR (600 MHz, $CDCl_3$) δ 8.02−7.98 (m, 2H), 7.63 (s, 1H), 7.51−7.43 (m, 9H).

*2-Chloro-1-morpholinoethan-1-one (**28**).* To a stirred solution of morpholine (435 mg, 4.99 mmol) in anhydrous THF (14 mL), K_2CO_3 (1.88 g, 10 mmol) was introduced. The reaction mixture was cooled to 0 °C, and $ClCH_2COCl$ (678 mg, 6.00 mmol) dissolved in THF (3 mL) was added dropwise. The reaction was warmed to rt and stirred for 1 h. After filtration, the filtrate was evaporated affording the target compound as a viscous oil with 95% purity according to ^{1}H NMR spectroscopy (620 mg, 76%). ^{1}H NMR (600 MHz, $CDCl_3$) δ 4.08 (s, 2H), 3.78−3.72 (m, 4H), 3.66−3.62 (m, 2H), 3.56−3.52 (m, 2H).

Biological Assays. *Compounds and PB1 Peptide.* RBV (1-D-ribofuranosyl-1,2,4-triazole-3-carboxamide) and oseltamivir carboxylic acid, the active form of oseltamivir [(3*R*,4*R*,5*S*)-4-acetamido-5-amino-3-(1-ethylpropoxy)-1-cyclohexene-1-carboxylic acid] were purchased from Roche. Test compounds were dissolved in dimethyl sulfoxide (DMSO). Since photochemical degradation of compound **12** under daylight conditions was observed during compound synthesis, all solutions containing **12** were protected from daylight, and all experiments with this compound were performed in the dark. The $PB1_{(1-15)}$-Tat peptide was synthesized and purified by the Peptide Facility of CRIBI Biotechnology Center (University of Padua, Italy). This peptide contains the first 15 N-terminal amino acids of PB1 protein fused to the C-terminal sequence of HIV Tat protein (amino acids 47−59).

Plasmids. Plasmids pcDNA−PB1, pcDNA−PB2, pcDNA−PA, and pcDNA−NP, containing cDNA copies of the influenza A/PR/8/34 virus *PB1*, *PB2*, *PA*, and *NP* genes, respectively, were created as described elsewhere[53] and kindly provided by P. Digard (Roslin Institute, University of Edinburgh, United Kingdom). Plasmid pPolI−Flu−ffLuc, which contains an influenza virus-based luciferase minireplicon vRNA under the control of the human RNA polymerase I promoter, was provided by L. Tiley (University of Cambridge, United Kingdom). Plasmid pRL−SV40 expressing the *Renilla* luciferase was purchased from Promega.

Cells and Virus. Human embryonic kidney 293T (HEK 293T) and MDCK cells were cultivated in Dulbecco's modified Eagle's medium (DMEM, Life Biotechnologies) supplemented with 10% (v/v) fetal bovine serum (FBS, Life Technologies) and antibiotics (100 U/mL penicillin and 100 μg/mL streptomycin, Life Technologies). The cells were maintained at 37 °C in a 5% CO_2 humidified atmosphere. Influenza A/PR/8/34 virus (PR8 strain, H1N1, Cambridge lineage) was obtained from P. Digard (Roslin Institute, University of Edinburgh, United Kingdom).

PA−PB1 Interaction Enzyme-Linked Immunosorbent Assay (ELISA). The PA−PB1 interaction was detected as described by Muratore et al.,[29] with some modifications. Briefly, microtiter plates (Nuova Aptca) were incubated with 400 ng of 6His-$PA_{(239-716)}$ for 3 h at 37 °C and then blocked with 2% BSA (Sigma) in PBS for 1 h at 37 °C. After washing, 200 ng of GST-$PB1_{(1-25)}$ dissolved in PBS, or GST as a control, in the presence of test compounds at various concentrations or DMSO, were added and incubated overnight at

DOI: 10.1021/acs.jmedchem.5b01935
J. Med. Chem. 2016, 59, 2688−2703

room temperature. *E. coli*-expressed, purified 6His-$PA_{(239-716)}$, GST, and GST-$PB1_{(1-25)}$ proteins were obtained as previously described.[29,54] After washing, the interaction between 6His−$PA_{(239-716)}$ and GST−$PB1_{(1-25)}$ was detected with an anti-GST monoclonal antibody conjugated to horseradish peroxidase (HRP) (Gen-Script). After the final wash step, the substrate 3,3′,5,5′-tetramethylbenzidine (TMB, KPL) was added, and the optical density was determined at 450 nm by an ELISA plate reader (Tecan Sunrise). Values obtained from the samples treated with only DMSO were used to set as 100% of PA−PB1 interaction. The $PB1_{(1-15)}$-Tat peptide was included in all experiments as the reference inhibitor.

In the modified PA−PB1 interaction ELISA, the assay was performed as described above, except that GST-$PB1_{(1-25)}$, or GST as a control, along with test compounds at various concentrations or DMSO were dissolved in serum-free DMEM instead of PBS. The $PB1_{(1-15)}$-Tat peptide was included in all experiments as a positive control for inhibition.

Plaque Reduction Assay (PRA). A confluent monolayer of MDCK cells was prepared in 12-well plates. Cells were infected with FluA virus (PR8 strain) at 40 PFU/well in DMEM supplemented with 1 μg/mL of TPCK-treated trypsin (Worthington Biochemical Corporation) and 0.14% BSA in the presence of various concentrations of test compounds for 1 h at 37 °C. Medium containing 1 μg/mL of TPCK-treated trypsin, 0.14% BSA, 1.2% Avicel, and test compounds at the same concentrations was then added. After 2 days of incubation, cell monolayers were fixed with 4% formaldehyde and stained with 0.1% toluidine blue, and viral plaques were counted. Ribavirin and Oseltamivir were included in all experiments as reference compounds.

Cytotoxicity Assay. Cytotoxicity of test compounds was assessed in MDCK and HEK 293T cells by the 3-(4,5-dimethylthiazol-2-yl)-2,5-diphenyltetrazolium bromide (MTT) method, as previously reported.[29,55] Briefly, MDCK cells (5×10^3 cells/well on 96-well plates) and HEK 293T (2×10^4 cells/well on 96-well plates) cells were incubated with compound at 2-fold serial dilutions from 250 μM. After 24 or 48 h for HEK 293T and MDCK cells, respectively, MTT solution (5 mg/mL in PBS) was added to each well, and plates were incubated for 4 h at 37 °C. Then, a solubilization solution was added to lyse cells. After 3 h of further incubation at 37 °C, absorbance was read at 620 nm using an ELISA plate reader (Tecan Sunrise). Values obtained from the wells treated with only DMSO were used to set as 100% of viable cells.

Minireplicon Assay. HEK 293T cells were seeded at a density of 2×10^5 per well into 24-well plates. After 24 h, cells were transfected with pcDNA-PB1, pcDNA-PB2, pcDNA-PA, and pcDNA-NP plasmids (100 ng/well of each) along with pPolI-Flu-ffLuc plasmid (50 ng/well). The transfection mixture also contained pRL-SV40 plasmid (50 ng/well) to normalize variations in transfection efficiency. Transfections were performed using calcium phosphate protocol in the presence of the test compounds or DMSO. Cell medium was replaced 4 h post-transfection with DMEM containing compounds or DMSO. At 24 h post-transfection, cells were harvested and both firefly luciferase and *Renilla* luciferase expression were determined using the Dual Luciferase Assay Kit from Promega. Ribavirin was included in all experiments as the reference compound.

Interference Compounds Assessment. The structure of all tested compounds (**1**−**15**) was examined for known classes of assay interference compounds with the online FAF-Drug^3 (Free ADME-Tox Filtering Tool) program.[56] Almost all the compounds passed the Pan Assay Interference Compounds (PAINS)[57] filter, increasing the confidence in the presented results. Only compound **6** failed to pass the PAINS filter. However, since this molecule did not display good activity in any of the performed *in vitro* assays, no further investigations were performed.

■ ASSOCIATED CONTENT

Supporting Information

The Supporting Information is available free of charge on the ACS Publications website at DOI: 10.1021/acs.jmedchem.5b01935.

Superposition of the PAC−PB1 homology model used in this study and the corresponding part of PDB ID 4WSB (Figure S1), binding mode of compounds **11**, **14**, and **15** predicted by the docking simulation (Figure S2), and the HSQC (Figure S3) and HMBC (Figure S4) spectra for compound **1** (PDF)

SMILES data (CSV)

■ AUTHOR INFORMATION

Corresponding Authors

*(M.B.) Phone: + 39 0557 2343306. Fax: +39 0577 234303. E-mail: botta.maurizio@gmail.com.

*(A.L.) Phone: +39 049 8272363. Fax: +39 049 8272355. E-mail: arianna.loregian@unipd.it.

Present Addresses

▽(M.B.) Dipartimento di Biotecnologie, Chimica e Farmacia, Università degli Studi di Siena, Via A. Moro, I-53100 Siena, Italy.

○(A.L.) Dipartimento di Medicina Molecolare, Università degli Studi di Padova, Via A. Gabelli 63, I-35121 Padova, Italy.

Author Contributions

#I.M.L.T., G.N. and A.L., M.B. contributed equally to this work, respectively.

Notes

The authors declare no competing financial interest.

■ ACKNOWLEDGMENTS

We gratefully acknowledge financial support provided by FP7 FLUCURE (ref. 259972) project to M.B. and by the University of Padua (Progetto di Ricerca di Ateneo 2014, grant no. CPDA141311 and Ex60%) to A.L. We would like to thank Maarten Sijm, Esther Reijnders, and Lorena van Gestel for technical assistance, P. Digard for providing plasmids pcDNA−PB1, pcDNA−PB2, pcDNA−PA, and pcDNA−NP as well as influenza A A/PR/8/34 virus (PR8 strain, H1N1, Cambridge lineage), and L. Tiley for providing the plasmid pPolI−Flu−ffLuc.

■ ABBREVIATIONS USED

FluA, influenza A virus; HA, hemagglutinin; NA, neuraminidase; CNS, central nervous system; RdRp, RNA-dependent RNA polymerase; PA, polymerase acidic protein; PB1, polymerase basic protein 1; PB2, polymerase basic protein 2; PPI, protein−protein interaction inhibitors; MWO, microwave oven; SAR, structure−activity relationship; ELISA, enzyme-linked immunosorbent assay; PRA, plaque reduction assay; MDCK, Mardin−Darby canine kidney; HEK, human embryonic kidney; RBV, ribavirin; DMEM, Dulbecco's Modified Eagle's Medium; SD, standard deviation; PAINS, pan assay interference compounds; PDB, Protein Data Bank; PAC, C-terminal portion of PA; PB1N, N-terminal portion of PB1; MD, molecular dynamics; RMSD, root mean square deviation; RMSF, root mean square fluctuations

■ REFERENCES

(1) WHO. Influenza (seasonal). Fact Sheet 211 March 2014. http://www.who.int/mediacentre/factsheets/fs211/en/ (accessed December 2015).

(2) Palese, P.; Shaw, M. L. Orthomyxoviridae: the Viruses and their Replication. In *Fields Virology*, 5th ed.; Fields, B. N., Knipe, D. M., Howley, P. M., Eds.; Lippincott Williams and Wilkins: Philadelphia, PA, 2007; pp 1647−1690.

DOI: 10.1021/acs.jmedchem.5b01935
J. Med. Chem. 2016, 59, 2688−2703

(3) Hilleman, M. R. Realities and Enigmas of Human Viral Influenza: Pathogenesis, Epidemiology and Control. *Vaccine* **2002**, *20*, 3068−3087.
(4) Suzuki, Y. Sialobiology of Influenza: Molecular Mechanism of Host Range Variation of Influenza Viruses. *Biol. Pharm. Bull.* **2005**, *28*, 399−408.
(5) Tong, S.; Zhu, X.; Li, Y.; Shi, M.; Zhang, J.; Bourgeois, M.; Yang, H.; Chen, X.; Recuenco, S.; Gomez, J.; Chen, L. M.; Johnson, A.; Tao, Y.; Dreyfus, C.; Yu, W.; McBride, R.; Carney, P. J.; Gilbert, A. T.; Chang, J.; Guo, Z.; Davis, C. T.; Paulson, J. C.; Stevens, J.; Rupprecht, C. E.; Holmes, E. C.; Wilson, I. A.; Donis, R. O. New World Bats Harbor Diverse Influenza A Viruses. *PLoS Pathog.* **2013**, *9*, e1003657.
(6) FLU.gov. http://www.flu.gov/pandemic/history/ (accessed December 2015).
(7) Centres for Disease Control and Prevention. http://www.cdc.gov/flu/pandemic-resources/index.htm (accessed December 2015).
(8) Mills, C. E.; Robins, J. M.; Lipsitch, M. Transmissibility of 1918 Pandemic Influenza. *Nature* **2004**, *7019*, 904−906.
(9) Belshe, R. B. The Origins of Pandemic Influenza-Lessons from the 1918 Virus. *N. Engl. J. Med.* **2005**, *353*, 2209−2211.
(10) Donaldson, L. J.; Rutter, P. D.; Ellis, B. M.; Greaves, F. E. C.; Mytton, O. T.; Pebody, R. G.; Yardley, I. E. Mortality from Pandemic A/H1N1 2009 Influenza in England: Public Health Surveillance Study. *BMJ.* **2009**, *339*, b5213.
(11) WHO. Overview of the Emergence and Characteristics of the Avian Influenza A (H7N9) Virus. 31 May 2013. http://www.who.int/influenza/human_animal_interface/influenza_h7n9/WHO_H7N9_review_31May13.pdf?ua=1 (accessed December 2015).
(12) Carrat, F.; Flahault, A. Influenza Vaccine: The challenge of Antigenic Drift. *Vaccine* **2007**, *25*, 6852−6862.
(13) Webby, R. J.; Webster, R. G. Are We Ready for Pandemic Influenza? *Science* **2003**, *302*, 1519−1522.
(14) Gasparini, R.; Amicizia, D.; Lai, P. L.; Brabazzi, N. L.; Panatto, D. Compounds with Anti-Influenza Activity: Present and Future of Strategies for the Optimal Treatment and Management of Influenza. Part I: Influenza Life-cycle and Current Available Drugs. *J. Prev. Med. Hyg.* **2014**, *55*, 69−85.
(15) Loregian, A.; Mercorelli, B.; Nannetti, G.; Compagnin, C.; Palù, G. Antiviral Strategies Against Influenza Virus: Towards New Therapeutic Approaches. *Cell. Mol. Life Sci.* **2014**, *71*, 3659−3683.
(16) Pielak, R. M.; Chou, J. J. Flu Channel Drug Resistance: a Tale of Two sites. *Protein Cell* **2010**, *1*, 246−258.
(17) Collins, P. J.; Haire, L. F.; Lin, Y. P.; Liu, J.; Russel, R. J.; Walker, P. A.; Skehel, J. J.; Martin, S. R.; Hay, A. J.; Gamblin, S. J. Crystal Structures of Oseltamivir-Resistant Influenza virus Neuraminidase Mutants. *Nature* **2008**, *453*, 1258−1261.
(18) Samson, M.; Pizzorno, A.; Abed, Y.; Boivin, G. Influenza Virus Resistance to Neuraminidase Inhibitors. *Antiviral Res.* **2013**, *98*, 174−185.
(19) York, A.; Fodor, E. Biogenesis, Assembly, and Export of Viral Messenger Ribonucleoproteins in the Influenza A Virus Infected Cell. *RNA Biol.* **2013**, *10*, 1274−1282.
(20) Obayashi, E.; Yoshida, H.; Kawai, F.; Shibayama, N.; Kawaguchi, A.; Nagata, K.; Tame, J. R. H.; Park, S. Y. The Structural Basis for an Essential Subunit Interaction in Influenza Virus RNA Polymerase. *Nature* **2008**, *454*, 1127−1131.
(21) He, X.; Zhou, J.; Bartlam, M.; Zhang, R.; Ma, J.; Lou, Z.; Li, X.; Li, J.; Joachimiak, A.; Zeng, Z.; Ge, R.; Rao, Z.; Liu, Y. Crystal Structure of the Polymerase PA_C-$PB1_N$ Complex From an Avian Influenza H5N1 Virus. *Nature* **2008**, *454*, 1123−1126.
(22) Resa-Infante, P.; Jorba, N.; Coloma, R.; Ortín, J. The Influenza Virus RNA Synthesis Machine: Advances in its Structure and Function. *RNA Biol.* **2011**, *8*, 207−215.
(23) Pflug, A.; Guilligay, D.; Reich, S.; Cusack, S. Structure of Influenza A Polymerase Bound to the Viral RNA Promoter. *Nature* **2014**, *516*, 355−360.
(24) Ortín, J.; Martín-Benito, J. The RNA Machinery of Negative-Stranded RNA Viruses. *Virology* **2015**, *479−480*, 532−544.
(25) Loregian, A.; Marsden, H. S.; Palù, G. Protein-Protein Interactions as Targets for Antiviral Chemotherapy. *Rev. Med. Virol.* **2002**, *12*, 239−262.
(26) Loregian, A.; Palù, G. Disruption of Protein-Protein Interactions: Towards New Targets for Chemotherapy. *J. Cell. Physiol.* **2005**, *204*, 750−762.
(27) Palù, G.; Loregian, A. Inhibition of Herpesvirus and Influenza Virus Replication by Blocking Polymerase Subunit Interactions. *Antiviral Res.* **2013**, *99*, 318−327.
(28) Fukuoka, M.; Minakuchi, M.; Kawaguchi, A.; Nagata, K.; Kamatari, Y. O.; Kuwata, K. Structure-Based Discovery of Anti-Influenza Virus A Compounds Among Medicines. *Biochim. Biophys. Acta, Gen. Subj.* **2012**, *1820*, 90−95.
(29) Muratore, G.; Goracci, L.; Mercorelli, B.; Foeglein, Á.; Digard, P.; Cruciani, G.; Palù, G.; Loregian, A. Small Molecule Inhibitors of Influenza A and B Viruses that Act by Disrupting Subunit Interactions of the Viral Polymerase. *Proc. Natl. Acad. Sci. U. S. A.* **2012**, *109*, 6247−6252.
(30) Muratore, G.; Mercorelli, B.; Goracci, L.; Cruciani, G.; Digard, P.; Palù, G.; Loregian, A. The Human Cytomegalovirus Inhibitor AL18 also Possesses Activity Against Influenza A and B Viruses. *Antimicrob. Agents Chemother.* **2012**, *56*, 6009−6013.
(31) Kessler, U.; Castagnolo, D.; Pagano, M.; Deodato, D.; Bernardini, M.; Pilger, B.; Ranadheera, C.; Botta, M. Discovery and Synthesis of Novel Benzofurazan Derivatives as Inhibitors of Influenza A Virus. *Bioorg. Med. Chem. Lett.* **2013**, *23*, 5575−5577.
(32) Massari, S.; Nannetti, G.; Goracci, L.; Sancineto, L.; Muratore, G.; Sabatini, S.; Manfroni, G.; Mercorelli, B.; Cecchetti, V.; Facchini, M.; Palù, G.; Cruciani, G.; Loregian, A.; Tabarrini, O. Structural Investigation of Cycloheptathiophene-3-carboxamide Derivatives Targeting Influenza Virus Polymerase Assembly. *J. Med. Chem.* **2013**, *56*, 10118−10131.
(33) Lepri, S.; Nannetti, G.; Muratore, G.; Cruciani, G.; Ruzziconi, R.; Mercorelli, B.; Palù, G.; Loregian, A.; Goracci, L. Optimization of Small-Molecule Inhibitors of Influenza Virus Polymerase: from Thiophene-3-carboxamide to Polyamido Scaffolds. *J. Med. Chem.* **2014**, *57*, 4337−4350.
(34) Pagano, M.; Castagnolo, D.; Bernardini, M.; Fallacara, A. L.; Laurenzana, I.; Deodato, D.; Kessler, U.; Pilger, B.; Stergiou, L.; Strunze, S.; Tintori, C.; Botta, M. The Fight Against the Influenza A Virus H1N1: Synthesis, Molecular Modelling, and Biological Evaluation of Benzofurazan Derivatives as Viral RNA Polymerase Inhibitors. *ChemMedChem* **2014**, *9*, 129−150.
(35) Tintori, C.; Laurezana, I.; Fallacara, A. L.; Kessler, U.; Pilger, B.; Stergiou, L.; Botta, M. High-throughput Docking for the Identification of New Influenza A Virus Polymerase Inhibitors Targeting the PA-PB1 Protein-protein Interaction. *Bioorg. Med. Chem. Lett.* **2014**, *24*, 280−282.
(36) Massari, S.; Nannetti, G.; Desantis, J.; Muratore, G.; Sabatini, S.; Manfroni, G.; Mercorelli, B.; Cecchetti, V.; Palù, G.; Cruciani, G.; Loregian, A.; Goracci, L.; Tabarrini, O. A Broad Anti-influenza Hybrid Small Molecule That Potently Disrupts the Interaction of Polymerase Acidic Protein−Basic Protein 1 (PA-PB1) Subunits. *J. Med. Chem.* **2015**, *58*, 3830−3842.
(37) Wunderlich, K.; Mayer, D.; Ranadheera, C.; Holler, A. S.; Mänz, B.; Martin, A.; Chase, G.; Tegge, W.; Frank, R.; Kessler, U.; Schwemmle, M. Identification of a PA-binding Peptide with Inhibitory Activity Against Influenza A and B Virus Replication. *PLoS One* **2009**, *4*, e7517.
(38) Sidwell, R. W.; Huffman, J. H.; Khare, G.; Allen, L. B.; Witkowsky, J. T.; Robins, R. K. Broad Spectrum Antiviral Activity of Virazole: I-Beta-D-ribofuranosyl-1,2,4-triazole-3-carboxamide. *Science* **1972**, *177*, 705−706.
(39) Ward, P.; Small, I.; Smith, J.; Suter, P.; Dutkowski, R. Oseltamivir (Tamiflu) and Its Potential for Use in the Event of an Influenza Pandemic. *J. Antimicrob. Chemother.* **2005**, *S1*, i5−i21.
(40) *Glide*, version 6.2; Schrödinger, LLC: New York, 2014.

DOI: 10.1021/acs.jmedchem.5b01935
J. Med. Chem. 2016, 59, 2688−2703

(41) Verdonk, M. L.; Cole, J. C.; Hartshorn, M. J.; Murray, C. W.; Taylor, R. D. Improved Protein−Ligand Docking using GOLD. *Proteins: Struct., Funct., Bioinf.* **2003**, *52*, 609−623.
(42) *Desmond Molecular Dynamics System*, version 3.7; D. E. Shaw Research: New York, 2014.
(43) Loregian, A.; Palù, G. How Academic Labs Can Approach the Drug Discovery Process as a Way to Synergize with Big Pharma. *Trends Microbiol.* **2013**, *21*, 261−264.
(44) *Prime*, version 3.0; Schrödinger, LLC: New York, 2011.
(45) *The PyMOL Molecular Graphics System*, Version 1.7.0; Schrödinger, LLC: New York.
(46) McWilliam, H.; Li, W.; Uludag, M.; Squizzato, S.; Park, Y. M.; Buso, N.; Cowley, A. P.; Lopez, R. Analysis Tool Web Services from the EMBL-EBI. *Nucleic Acids Res.* **2013**, *41*, W597−600.
(47) *Maestro*, version 9.7; Schrödinger, LLC: New York, 2014.
(48) *LigPrep*, version 2.9; Schrödinger, LLC: New York, 2014.
(49) Mekheimer, R. Synthesis of Aminopyridines from Azidopyridines and Tetrazolo[1,5-a] Pyridines. *Pharmazie* **1994**, *49*, 322−324.
(50) Schomaker, J. M.; Delia, T. J. Arylation of Halogenated Pyrimidines via a Suzuki Coupling Reaction. *J. Org. Chem.* **2001**, *66*, 7125−7128.
(51) Abdel-Fattah, A. M.; Elneairy, M. A. A.; Gouda, M. N.; Attaby, F. A. Synthesis, Characterization, and Reactions of Pyridine-3-Carbonitrile Derivatives. *Phosphorus, Sulfur Silicon Relat. Elem.* **2008**, *183*, 1592−1614.
(52) Carles, L.; Narkunan, K.; Penlou, S.; Rousset, L.; Bouchu, D.; Ciufolini, M. A. 2-Pyridones from Cyanoacetamides and Enecarbonyl Compounds: Application to the Synthesis of Nothapodytine B. *J. Org. Chem.* **2002**, *67*, 4304−4308.
(53) Mullin, A. E.; Dalton, R. M.; Amorim, M. J.; Elton, D.; Digard, P. Increased Amounts of the Influenza Virus Nucleoprotein do not Promote Higher Levels of Viral Genome Replication. *J. Gen. Virol.* **2004**, *85*, 3689−3698.
(54) Loregian, A.; Appleton, B. A.; Hogle, J. M.; Coen, D. M. Residues of Human Cytomegalovirus DNA Polymerase Catalytic Subunit UL54 that are Necessary and Sufficient for Interaction with the Accessory Protein UL44. *J. Virol.* **2004**, *78*, 158−167.
(55) Loregian, A.; Coen, D. M. Selective anti-cytomegalovirus compounds discovered by screening for inhibitors of subunit interactions of the viral polymerase. *Chem. Biol.* **2006**, *13*, 191−200.
(56) FAF-Drugs^3 Free ADME/tox Filtering tool 3, version June 2015. http://fafdrugs3.mti.univ-paris-diderot.fr (accessed December 2015).
(57) Baell, J. B.; Holloway, G. A. New Substructure Filters for Removal of Pan Assay Interference Compounds (PAINS) from Screening Libraries and for Their Exclusion in Bioassays. *J. Med. Chem.* **2010**, *53*, 2719−2740.

DOI: 10.1021/acs.jmedchem.5b01935
J. Med. Chem. 2016, 59, 2688−2703